TIDAL IIISRUPTION AND THE APPEARANCE OF PERIODIC COMET SHOEMAKER-LEVY 9

Zdenek Sekanina, Paul W. Chodas, and Donald K. Yeomans

Jet Propulsion Laboratory, California Institute of Technology
Pasadena, CA 91109, U. S. A.

Submitted to *The Astronomical Journal*

November 1993

Abstract

A unified model is presented that quantitatively interprets the observed characteristics of the nuclear train, the two dust trails, and the tail region of P/Shoemaker-Levy 9 in terms of a collisionally modified rotation velocity distribution of the comet's debris. The disruption of the parent comet was due primarily to tidal stresses during its extremely close approach to Jupiter in July 1992. The original nucleus is found to have been at least ~4.5 km in radius or, equivalently, $\sim 10^{17}$ g in mass, The dynamical separation of the debris occurred most probably ~1.5 hr after the perijove passage, even though the actual fragmentation of the original mass is likely to have begun before closest approach. Physical breakup was accompanied by ubiquitous low-velocity collisions among the particulates, resulting in a rearrangement of the initial rotational velocities into a rapidly "thermalized" distribution, characterized by a long tail of relatively high velocities for centimeter-sized and smaller fragments. The period of intense particle-particle collisions is estimated to have continued for at least ~0.1 day, at which time the radial differential perturbations by Jupiter and orbital-velocity differences began to dominate the relative motions of the debris. The particle mass distribution appears to be fairly flat, $\propto m^{-1} dm$, for centimeter-sized and larger fragments, but steeper than $m^{-2} dm$ for the microscopic. debris. The fine dust contributes much of the total observed cross-sectional area, but its share of the total mass of the assemblage is negligible. The effective radii of the 21 largest fragments range from <1 km to >2 kin, based 011 Weaver *et al.*'s (1993) results and 011 constraints implied by our model. The debris populating the west- southwestern trail appears to be predominantly pebble. and boulder-sized, while the debris in the east-northeastern trail is mostly subcclltiII~etcI-sized, The diffuse sector to the north of the trails (including the tails of the individual fragments) consists primarily of microscopic dust, subjected to appreciable effects of solar radiation pressure. Predictions are presented for the projected lengths and position angles of the nuclear train, the dust trails, and the tail region between mid-December 1993 and mid-July 1994. Also predicted are projected separations of the 21 nuclei and estimates for the impact times and other circumstances of the comet's encounter with Jupiter in 1994.

1. 1N'1'1LODUC7'1ON: TI II; CURRENT STATUS

The aim of this investigation is to interpret the unique appearance of Periodic Cornet Shoemaker- Levy 9 and to understand the object 's history and especially the circumstances of its breakup at the time of its exceptionally close approach to Jupiter on 8 July 1992. The comet's observed appearance (Fig. 1), which has not changed dramatically since discovery in late March 1993, can be described as follows: (i) the most spectacular feature is a *train* of as many as 21 nuclei, which line up al most perfectly in a direction from the cast-northeast to the west-southwest; the train's length had increased from ~50 arcsec at discovery to ~70 arcsec by mid-July of 1993; (ii) extending from the nuclear train on either side arc *dust trails*, the west-southwestern branch having been reported as consistently the longer of the two and aligned perfectly (within errors of observation) with the nuclear train; the cast-northeastern branch appears to be slightly bent relative to the nuclear train, making an angle with the cast-west direction about 4° greater than that of the nuclear train and the west-southwcstcml trail; (iii) the nuclear train and the two trails make up a boundary of an enormous sector of material that stretches to the north of it, gradually fading out; the wide section of this feature that is outside the nuclear train appears to be virtually structureless, but the band of debris that issues from the nuclear train displays a set of parallel, fairly narrow *tails* that extend to the west-northwest and whose roots can be identified with some of the individual nuclei.

Scotti and Melosh (1993) have proposed that the cornet's tidal disruption was due en - tirely to radial differential perturbations by Jupiter, and found that the observed temporal variations in the apparent length and orientation of the nuclear train can be predicted 011 the assumption that the breakup occurred exactly at closest approach to J upiter and that the implied nuclear diameter of the progenitor comet was ~2 km. This result is inconsistent with the dimensions of the comet's fragments determined photometrically from observations made with the Hubble Space Telescope (Weaver *et al.* 1993). On certain assumptions, the brightest fragment was found to have an equivalent diameter of 4.3 km and 10 others diameters between 2.5 and 3.9 km. The equivalent diameter of a sphere that would contain the mass of these 11 fragments alone is already ~8 km. Accounting for additional contributions from the remaining nuclei and from the large amounts of dust, one obtains a more probable estimate of 9 km for the nuclear diameter of the parent comet, which is a factor of almost 5 greater than Scotti and Melosh's dynamically derived value. To explain this discrepancy, the brightness of each fragment would have to be overestimated by more than 3 magnitudes or the geometric albedo underestimated by a factor of 20 or more! While Weaver *et al.* have remarked that the derived nuclear magnitudes may not be entirely free from residual dust contamination in the central pixel, the effect is rather insignificant.

The inconsistency between the two estimates could be removed by postulating a highly elongated shape of the original nucleus ant] assuming that the photometric results refer to its maximum cross section and the dynamical information to its minimum dimension. However, this *ad hoc* explanation cannot be upheld, since it requires that the parent comet's nucleus split along its shortest (and therefore the least likely) body axis and that *all* 11 photometrically measured nuclei projected their maximum cross-sectional areas toward Earth at the same time. Rather than subscribing to such a vulnerable hypothesis, we have searched for alternative dynamical solutions that would be more in line with the evidence presented by Weaver *et al.* (1993).

2. IMPROVED ORBIT DETERMINATION

Both the model development and the comet's highly probable collision with Jupiter in late July 1994 give a certain urgency to the efforts to compute accurately this object's orbit and predict its future motion. Unfortunately, computations to determine the orbital characteristics of P/Shoemaker-Levy 9 have been hampered try a lack of astrometric information pertaining to the individual nuclei. Almost all the absolute astrometric data received to date refer to the midpoint of the nuclear train and this position is not necessarily the comet's center of mass. '1'able 1 presents the heliocentric and jovicentric orbits for the comet based upcm 157 astrometric positions spanning the interval from 1993 March 17 through July 11. Although the comet is in a loosely bound orbit about Jupiter, the orbit is first computed in the heliocentric reference frame (J2000) and then converted to the jovicentric reference frame. It is this latter frame that is employed in the subsequent analysis. The JPL planetary ephemeris DE200 (Standish 1990) has been used in our analysis. In the orbital solutions, the observed and computed positions are subtracted to form observation residuals and the initial orbital parameters are adjusted by a least squares differential correction process until the root-mean-square value of these residuals reaches a minimum. Because of the peculiar nature of the object's image and the confusion as to which point of the nuclear train was measured, many of the observations had to be eliminated as discordant. The final root-mean-square residual of the 157 retained observations is 1,37 arcsec. Because the cored is in a loose orbit about Jupiter, the perturbative accelerations from the Sun arc unusually large and the characteristics of the heliocentric and jovicentric orbits change constantly with time. The following osculating orbits arc appropriate only for the instant of the given epoch. The orbital data for the 21 individual nuclei based on their relative astrometric observations (J ewitt 1993, Weaver *et al.* 1993) required a special strategy and their analysis is postponed to Sec. 8.

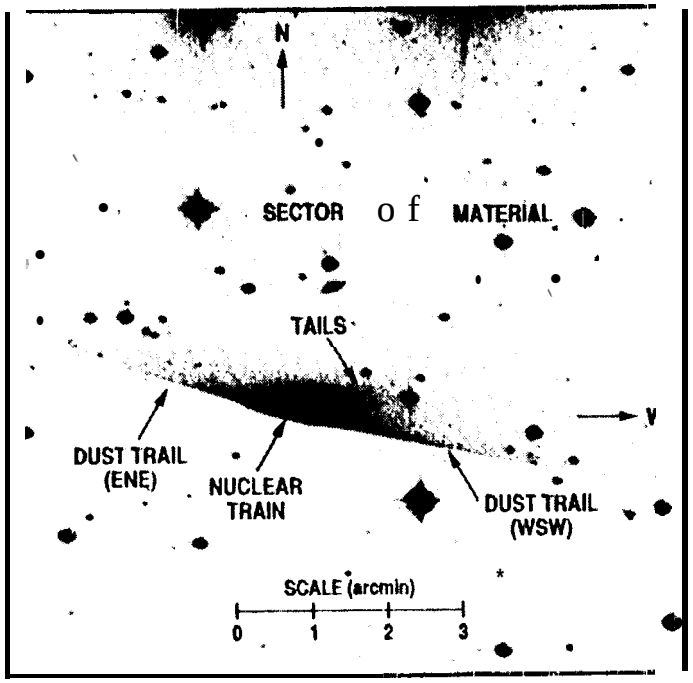

FIG. 1 image of Comet P/Shoemaker-Levy 9 based upon a 440 second exposure taken by J. V. Scotti with the University of Arizona's 91-cm Spacewatch telescope on March 30, 1993. The field is 9 arcmin on a side, with north up and east to the left. The nuclear train, the two dust trails, and the wide sector of material, with the multitude of narrow tails embedded, are marked. (Original courtesy of J. V. Scotti, Lunar & Planetary Laboratory.)

3. NUCLEAR TRAIN AND DUST-TRAIL DYNAMICAL CONSTRAINTS

A number of numerical integration runs were made to investigate the comet's motion about Jupiter. Each time beginning with the nominal jovicentric orbit represented in Table 1, we assumed that the comet tidally disrupted at or near the 1992 perijove time and numerically followed the comet's subsequent motion as it evolved under the influence of solar and planetary perturbations. For each numerical experiment, the comet's nominal orbit at the assumed time of disruption was varied by one or more components in its position or velocity vector.

As a check of our computations, we used the initial conditions and assumptions employed by Scotti and McIosh (1993) and closely reproduced their results. We then substituted our more recent initial orbit (Table 1) and continued the analysis. Assuming that the tidal disruption occurred exactly at the July 1992 perijove, we could reproduce the length and, approximately, the position angle of the nuclear train over a period of March 27-July 17, 1993, derived from high-precision positional data (Jewitt 1993, Weaver et al. 1993), by employing either a difference in the distance from the comet's center of mass of $\Delta r = 0.89$ km along the Jupiter- comet line or by introducing an impulse, in the direction of the orbital velocity, of $\Delta V_{orb} = 0.187$ m/s. Thus, in terms of the nuclear train observations, either a small radian separation of the fragments at disruption or their small velocity increment (or a combination thereof) would result in their same apparent evolution. On the other hand, none of the remaining initial position or velocity components had a measurable effect upon the evolution of the fragments in the train, as seen from Earth. We next varied the time of disruption, t_0, and found that it critically affected the results in a highly nonlinear fashion, as seen from Fig. 2. The curves can closely be reproduced by differential forms of the virial theorem, employing a quasi-parabolic approximation and assuming a spread of $\Delta P_J = 5.55$ days among the osculating jovicentric orbital periods of the fragments. The equivalent values of Δr (in km; at $\Delta V_{orb} = 0$) and of ΔV_{orb} (in m/s; at $\Delta r = 0$) are

TABLE 1. Orbital parameters for Periodic comet Shoemaker- Levy 9.

Heliocentric orbit (J2000 ecliptic reference frame)		
Epoch (TDB)	1993 Aug. 1.0	
Eccentricity	0.04989254:0.0002306	
Perihelion distance (All)	5.0028102 ± 0.0007084	
Perihelion time (TDB)	1997 Nov. 29,177775 ± 6.3198	
Argument of perihelion	32°.8878195 ± 0°.4651962	
Longitude of ascending node	297°.05377743 0°.0408877	
Inclination	1°.11056584 0°.0002375	
Jovicentric orbits (J2000 ecliptic reference frame)		
Epoch (TDB)	1992 July 8.0	1994 July 21.0
Eccentricity	0.9959494	0.9987037
Perijove distance (km)	112820.73	35721.56
Perijove time (TDB)	1992 July 8.01997	1994 July 2).21845
Argument of perijove	254°.47689	274°. 0G310
Longitude of ascending node	50'.65833	44°.75213
Inclination	63°.59388	76°.77102

[a] The errors are 1-0 formal solution uncertainties.

$$\Delta r(t_0)_{\Delta V_{orb}=0} = \left[\left(\frac{2\pi}{k_J}\right)^{2/3}\frac{q_J^2}{3P_J^{5/3}}\Delta P_J\right] z^2 = 0.89z^2,$$
$$\Delta V_{orb}(t_0)_{\Delta r=0} = \left[\frac{(2\pi)^{2/3}}{3\sqrt{2}}\frac{k_J^{1/3}\sqrt{q_J}}{P_J^{5/3}}10^3\Delta P_J\right]\sqrt{z} = 0.187\sqrt{z}, \quad (1)$$

where $k_J = 1.12564 \times 10^4\ km^{\frac{3}{2}}/s$ is the Gaussian gravitational constant for Jupiter, q_J and P_J are the comet's perijove distance (in km) and its jovicentric orbital period (in s) at the osculation time of July 8, 1992 (Table 1 and Sec. 2), and the dimensionless quantity z is the jovicentric distance at breakup in units of q_J. In a parabolic approximation, z is related to the time interval between breakup and perijove, $t_0 - T_J$ (in days) as follows:

$$|t_0 - T_J| = 0.018368\sqrt{z-1}\,(z+2), \quad z \geq 1. \quad (2)$$

For $t_0 = T_J$, we have, of course, $z = 1$, whereas for $t_0 = T_J \pm 0.05$, 0.10, 0.15, and 0.20 clay z is, respectively, 1.579, 2,478, 3.339, and 4.142.

There also is a small effect in the position angle of the train. For $t_0 = T_J$ the calculated position angle varies from 257.°5 in late March to 255.°5 in mid-July 1993 regardless of the assumed scenario. A change by + 0.1 clay in the time of breakup shifts the nuclear train orientation by up to --0.°5 in either approach (Δr or ΔV_{orb}). For a change by --0.1 day, the respective change is + 0.°5.

The above conclusions also largely apply to the dust trails, except that the separation effect is considerably greater. In order to ascertain existing observational constraints, we list, in Table 2, all information on the dust trails- as well as the tails- that we have been able either to find in the literature or to derive from available images. Inspection of the table shows that any interpretation should explain the trail extent, in late March 1993, of up to at least 10.5 arcmin in the west-southwestern direction and at least 6.2 arcmin in the

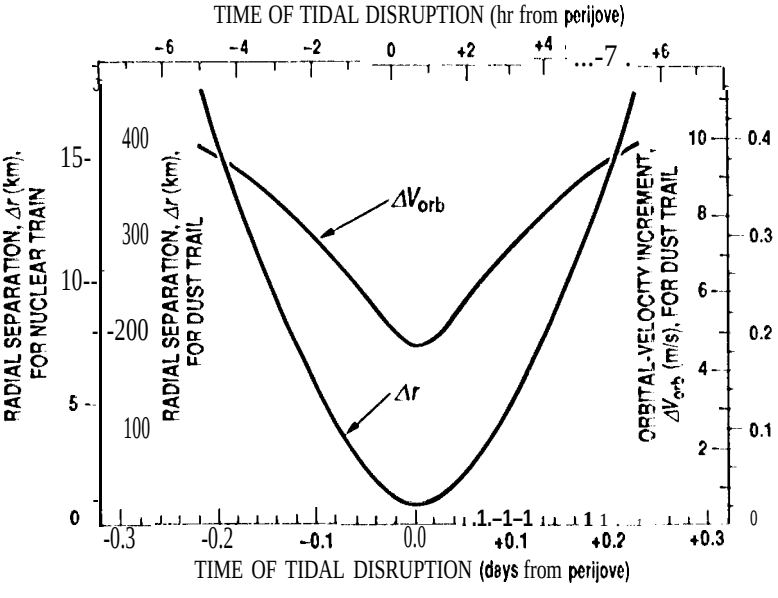

FIG. 2. Radial separation Δr at breakup (left scales) and the orbital-velocity increment ΔV_{orb} (right scales) vs. the time of breakup. All plotted values of Ar (for $\Delta V_{orb} = 0$) and A V_{orb} (for $\Delta r = 0$) satisfy the observed halflength of the nuclear train (outside scales) and the length of the west-southwestcml trail (inside scales).

east-northeastern direction. If the comet broke up exactly at perijove, the required radial separation for the west-southwesbmI trail is $\Delta r = +22$ km, whereas the orbital-velocity increment is $\Delta V_{orb} = +4.7$ m/s. For the east-northeastern trail the respective numbers are $\Delta r = -13$ km and $\Delta V_{orb} = -2.7$ m/s. For the debris that physically separated somewhat before or after the closest approach, much greater values of Δr or a little greater values of ΔV_{orb} arc required (Fig. 2). It is shown in this paper that even though the particle-rwlcasc mechanisms are different, the properties of dust in the trails of P/Shoemaker-Levy 9 arc similar to those of particulate material in the trails of several short-period comets (e.g., Sykes *et al.* 1990, Sykes and Walker 1992), which led us to accept the same terminology.

Dust particles released during the breakup ant] subsequently affected, to an appreciable degree, by solar radiation pressure were found to line up, from each "parent" fragment in the train, at a position angle of *280°* in late March, 270° in late May, and 2710 in mid-July] 993. Locations of dust particles subjected to radiation-pressure accelerations of 1 % of the solar attraction were between 0.6 and 0.9 arcmin from the nuclear train in late March through mid-July, with the minimum projected distance reached in May. Both the length and orientation of the tails arc insensitive to the time of breakup, We also calculated effects due to the light reflected from Jupiter and found them negligibly small.

The high correlation between the dispersion effects by the jovian radial perturbations on the one hand and by slight changes in the orbital velocity 011 the other is illustrated in Fig. 3, in which the nuclear-train solutions arc plotted for several assumed times Of disruption around the 1992 time of closest approach to Jupiter. This relationship, too, is predicted by the virial theorem. In a parabolic approximation, its form is:

TABLE 2. Observations of dust trails and tails of Periodic comet Shoemaker-Levy 9 (1993c).

	Dust trails						
	East-northeastern		West-southwestern		Tails		
Date 1993 (UT)	Length (arcmin)	Position angle	Length (arcmin)	Position angle	Length[a] (arcmin)	Position angle	Observer(s) & reference
Mar. 26.30	4.20	74"	6.89	260°	1.34	286°	Scotti (1993)
28.02	0.7	72	2.3	256	1	300	Cavagna *et al.* (1993)
28.24	3.96	72	≥4.37	258	1.21	285	Scotti (1993)
28.29		73[b]		258[b]			Wisniewski (1993)
30.31	6.16	75	10.43	260			Scotti (1 993)
31.2						292'	Helin (1993)
Apr. 1.71	2.9	77	3.4	258			Nakamura (Green 1993)
14.59	3.4	71	3.3	256			Nakamura (Green 1993)
14.63	2	70	5	255			Urata (1 993)
17.58	3.0	70	3.6	257			Nakamura (Green 1993)
25.52	2.3	74	4.8	256			Nakamura (Green 1993)
May 15.61	2.5	75	3.0	256			Nakamura (Green 1993)
17.84			10	~260			Mikuz (Green 1993)
20.61				255			Nakamura (Green 1993)
25.60			2.8	253			Nakamura (Green 1993)

[a] Applies to the tail of the brightest fragment.
[b] Measured by Z. Sekanina.
[c] Measured by Z. Sekanina and R. A. Bambery.

$$\Delta V_{\rm orb}(t_0) = A - B \cdot \Delta r(t_0), \tag{3}$$

where the coefficients A (in m/s) and B (in ln/s/km) are

$$A = \Delta V_{\rm orb}(t_0)_{\Delta r = 0} = 0.187\, z^{1/2},$$
$$B = \frac{\Delta V_{\rm orb}(t_0)}{\Delta r(t_0)}_{|\Delta r = 0} \cdot \cdot 0.210\, z^{-3/2}, \tag{4}$$
$$\Delta r(t_0)_{\Delta V_{\rm orb} = 0}$$

and z has the same meaning as in (1) and (2).

An obvious inference from the $(\Delta r, \Delta V_{\rm orb})$ correlation and its dependence on the time of disruption is that Scotti and Melosh's (1993) very tight constraint on the parent comet's nuclear size is suspect on dynamical grounds. We develop an approach that allows us to consider both sour-cm of dispersion effects and to interpret the tidal splitting as a time dependent process rather than a sudden event. This approach opens up an attractive opportunity for modeling the nuclear train, the dust trails, and the entire tail region as different manifestations of the breakup and as products of the same physical and dynamical conditions that accompanied it. These conditions arc, in part, detm-mined by (i) the parent comet's state of rotation at the time of breakup and (ii) the inevitable gravitational perturbations and collisions among individual pieces of the debris during a subsequent limited period of time. An important characteristic that describes the environment of these particle interactions is the velocity distribution of the debris. A crude estimate for

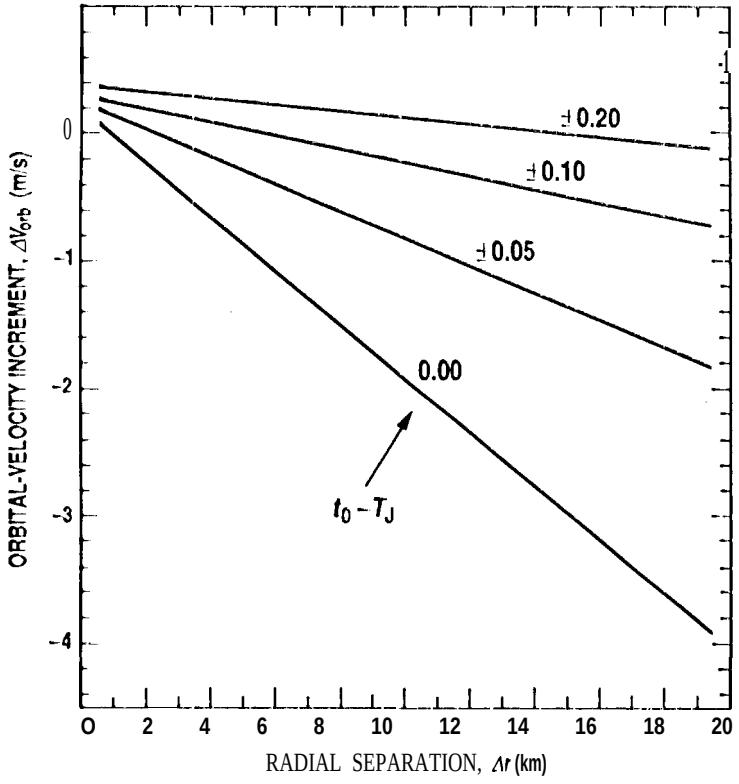

FIG. 3. Relationship between the radial separation Δr and the increment $\Delta V_{\rm orb}$ in the orbital velocity that satisfies the observed dispersion effects on the nuclear train, as a function of the time interval between breakup and perijove, t_0 -7 j (in days). For example, for a radial separation of 10 km at perijove $(t_0 - T_J = 0)$, the observations can only be represented with an orbital velocity increment of - 1.9 m/s.

an initial particle velocity is provided by the surface escape velocity, V_{esc}, which for a sphere of radius R (in km) and average bulk density p (in g/cm^3) amounts (in m/s) to

$$V_{esc} = 0.75\, R\sqrt{\rho}. \qquad (5)$$

Because of the extremely low cohesion strength indicated by the comet's tidal breakup (Sekanina 1993, Scotti and Melosh 1993), we prefer a low density of $\rho = 0.2$ g/cm^3, which for comets in general was also inferred from other evidence (e.g., Rickman 1986). This density yields $V_{esc} = 1$ m/s for a nucleus 3 km in radius and 0.23 x 10^{17} g in mass; and 2 m/s for a nucleus 6 km in radius and 1.8 x 10^{17} g in mass. On a rotating nucleus the escape velocity can be lower or higher than the value given by (5), depending on the direction of the released material (Dobrovolskis and Burns 1984). A rotationally unstable object, which spins with an equatorial velocity greater than the (appropriately corrected) escape velocity, has a rotation period shorter than the critical value of $P_{crit} = 3.30\ \rho^{-1/2}$ hr, equal to 7.38 hr at the above low density. It is obvious that in the course of tidal fracture the neighboring fragments of the parent nucleus are released with typical relative velocities that are only a small fraction of 1 m/s. In the following we distinguish between the nuclei, which we usually call *fragments* or *large fragments*, and the remaining dust material, which we call (*dust*) *particles* or *particulate debris* or just debris.

Since the axis of maximum tension is aligned with the radial direction to the perturbing planet, the tidal disruption will tend to proceed along the stress planes that are normal to the comet-planet line (Aggarwal and Oberbeck 1974; Dobrovolskis 1990). Disregarding the post-breakup interactions for a moment, we consider three particular rotation states for the original nucleus at the time of splitting that coincides with perijove. If the spin vector is in the orbital plane and oriented perpendicularly to the comet-Jupiter line at breakup, the rotation velocities of neither the large fragments nor the particulate debris in the trails will contribute to the transverse direction. Thus, the observed considerable extent of the trails cannot be explained, in terms of this highly idealized model, as a result of tidal fracture of an inactive comet nucleus. If the spin vector is normal to the orbital plane, the combined dispersion effects of Jupiter's radial differential perturbations and of the transverse component of the rotation velocity on the large fragments and the trail debris will be comparable. The difference in the extent of the nuclear train and the dust trails is thus once again not qualitatively understood. Consider next a scenario in which the spin vector points at Jupiter. Since the stress planes are now cut along the parallels of cometocentric latitude, the centers of mass of the large fragments will be located on (or, for an irregular nucleus, very near) the rotation axis and they will receive a rotational- but no translational- momentum at breakup. Thus, the dispersion effect on the large fragments will be due entirely to the differential perturbations, as assumed by Scotti and Melosh (1993). On the other hand, the rotation will impart some translational momentum in the transverse direction to the debris, except for particles distributed along the meridian that lies in the orbital plane at the time of splitting. In addition, all particles coming from locations outside the equatorial plane will be subjected to radial differential perturbations by Jupiter. Thus, of the three scenarios considered, only in this third one will there be a qualitative difference between the dispersion effects on the large fragments and on the particulate debris, Even without considering the post-breakup interactions, it is apparent that the spatial distributions of the tidal-fracture products will be affected by the progenitor comet's spill-vector orientation at the time of splitting.

4. EARLY EVOLUTION OF THE DEBRIS: GRAVITATIONAL AND COLLISIONAL INTERACTION

To illustrate the role of gravitational perturbations among the individual pieces of the debris immediately following the breakup, we compare the gravitational acceleration γ_f by a large fragment, of mass M_f, at a distance r_f,

$$\gamma_f = \frac{GM_f}{\quad}, \tag{6}$$

with Jupiter's differential gravitational acceleration $\Delta\gamma_J$ over a span Δr_J in the radial direction and at a distance r_J from the planet,

$$\Delta\gamma_J = \frac{2GM_J}{r_J^3}\Delta r_J, \tag{7}$$

where $G = 6.67 \times 10^{-8}\,\mathrm{cm^3/g/s^2}$ is the gravitation constant. Taking $M_J = 1.9 \times 10^{30}$ g, $r_J = 1.13 \times 10^5$ km (Table 1), and, for a large fragment, $M_f \simeq 10^{16}$ g, we find that the condition $\Delta\gamma_J \gg \gamma_f$ is satisfied only when $\Delta r_J >> 1.6$ km. Thus, the gravitational attraction by the large fragments is not entirely negligible in the early post-breakup period, especially not on particles for which the point of closest approach to such a fragment is located in or near the plane perpendicular to the comet-Jupiter direction, where $\Delta\gamma_J \simeq 0$.

To estimate the magnitude of an integrated effect by a large fragment, we consider a dust particle moving in a hyperbolic grazing orbit relative to the fragment. Since the escape velocity from any fragment is significantly lower than that from the original nucleus, it is likely that initial rotational velocities of some particles already exceed a fragment's escape velocity. It can be shown that, within a distance r_f from the fragment, the total change, ΔV, in the particle's velocity due to the encounter is

$$\Delta V(r_f) = \frac{2}{e}|\dot{r}_f|, \tag{8}$$

where $e > 1$ is the eccentricity of the grazing orbit. in the limit

$$\Delta V_\infty = \lim_{r_f \to \infty} \Delta V(r_f) = \frac{2V_\infty}{e}, \tag{9}$$

where V_∞ is the particle's pre-encounter velocity relative to the fragment '(at infinity.>' If V_{esc} is the surface escape velocity from the fragment and if we define

$$x = \frac{V_{esc}}{V_\infty}, \tag{10}$$

we have $e = 1 + 2/x^2$ and can write (9) in the form:

$$\Delta V_\infty = \frac{x}{1 + \frac{1}{2}x^2} V_{esc}. \tag{11}$$

The function of x reaches a maximum value at $x = \sqrt{2}$, when $V_\infty = V_{esc}/\sqrt{2}, c = 2$, and

$$\max(\Delta V_\infty) = \frac{V_{esc}}{\sqrt{2}}. \tag{12}$$

For the largest fragment of P/Shoemaker-Levy 9, for which Weaver et al. (1993) derived $2R$ = 4.3 km, Eq. (5) yields V_{esc} = **0.7** m/s when ρ ::"0.2 g/cm3 Thus, the velocity changes due to encounters among low-density fragments never exceed a fraction of I m/s. This is especially so, because the typical time scale on which most of the integrated effect of a single encounter occurs is fairly long, on the order of 0.1 day or more and there is no time for any particle to undergo many such encounters before the debris disperses in space. We show below that collisional lifetimes and mean free paths of the particulates are so short in the early phase of the debris evolution that no encounter event can be completed uninterrupted by the collisions, during which a particle's velocity changes stepwise on a time scale of a fraction of one second. Grazing encounters between two large fragments are even Icss likely because of the limited number of these objects. The resulting velocity changes ΔV_∞ arc also smaller than for the grazing encounters between a large fragment and a small particle, because of stronger constraints on the minimum distance between the centers of mass. These conclusions are consistent with the estimate of $\sim$0.2 m/s for the orbital-velocity increment that we established in Sec. 3 from the length of the nuclear train. On the other hand, the velocity dispersion of up to $\sim$5 m/s (at $\Delta r = 0$), derived from the length of the west-sout}lwcstcrll trai], does not appear to be an accumulated effect of fragment- particle grazing encounters and another mechanism is necessary for its explanation.

It is proposed that particle-particle collisions provide the answer, if their rate is high enough and their character helpful in building up the momentum for at least a fraction of the particle population, To address these issues, we consider a particle of radius s that, at a time t shortly after the splitting of the nucleus, moves with a velocity $V(t)$. During a time interval Δt it collides with $\pi(s+\langle s\rangle)^2 V(t)\Delta t \cdot N_0(t)$ target particles, where $N_0(t)$ is the spatial number density of the particulate debris at the time and $\langle s\rangle$ is a characteristic size of the targets. The particle's mean free path can be approximated by

$$\ell(t) = \frac{1}{\pi\left(s+\langle s\rangle\right)^2 N_0(t)}, \tag{13}$$

where the number density can be written as a ratio of the total number of particles, $N(t)$, and the volume of space they occupy, $\mathcal{U}(t)$. Assuming that, ever since discovery, the comet's dust cloud has been optically thin, the total cross-sectional area A of the debris can be approximated using the comet's total brightness. Calling $H_{norm}(t)$ the magnitude, at a time t, that is normalized to 1 AU from both Earth and the Sun by the inverse square law of geocentric and heliocentric distances, one has for $\mathcal{A}(t)$ (in km^2)

$$\mathcal{A}(t) = \frac{1.42\times 10^{6-0.4H_{norm}(t)}}{p}, \tag{14}$$

where p is an assumed geometric albedo of the particulate debris. As seen below, the results also depend on the assumed phase-effect correction.

A total of 30 consistent integrated-brightness estimates, obtained by 8 observers between March 26 and July 17, 1993, have been selected (Green 1993, Bortle 1993, Meyer *et al.* 1993, Scotti 1993) and converted into a standard visual-magnitude system. Two additional July data points, grossly inconsistent with each other, have been ignored. If the gradual decrease in $\mathcal{A}$ (Fig. 4) is due to a dwindling surface brightness of a slowly expanding dust cloud formed in the wake of disruption and newer replenished, the rate of decrease in the observed cross-sectional area, $d\mathcal{A}/dt$, will vary approximately as the instantaneous cross section $\mathcal{A}$, and the expected temporal dependence will follow a simple law:

$$\mathcal{A}(t) = \mathcal{A}_0 \exp\left[-\psi(t-t_0)\right], \tag{15}$$

when-c $\mathcal{A}_0$ is the true cross-sectional area of the debris and ψ is a constant. The rate of change in the normalized magnitude $H_{\rm norm}$ with time is then equal to $dH_{\rm norm}/dt = 1.086\psi$. In practice, uncertainties in determining $\mathcal{A}_0$ stem both from the necessity to extrapolate over more than 8 months Lack in time and from low accuracy of the brightness estimates. For an assumed geometric albedo of 0.04 and a phase effect of 0.035 mag/deg, least, squares solutions to the data points in Fig. 4 yield $H_{\rm norm}(t_0) = 2.58 \pm 0.22$, & $= 3.3^{+0.7}_{-0.6}$ million km^2, and $\psi = 0.0083 \pm 0.0007$/day, while $H_{\rm norm}(t_0) = 1.5130.24$, $\mathcal{A}_0 = 8.8^{+2.2}_{-1.7}$ million km^2, and $\psi = 0.0122 \pm 0.0008$/day when 110 phase correction is applied. The first option seems a more likely case, because it predicts the comet to have been of an apparent visual magnitude of $\sim$1 0.5 immediately following the breakup, whereas the other scenario would make it then just about magnitude 9 and thus Icss apt to escape detection at a time when Jupiter's elongation from the Sun still exceeded 50°.

The total number of particles in the cloud of debris can now be written in terms of the cross-sectional area do and the mean quadratic dust-particle radius $\langle s^2 \rangle^{1/2}$:

$$N = \frac{\mathcal{A}_0}{\pi \langle s^2 \rangle}. \tag{16}$$

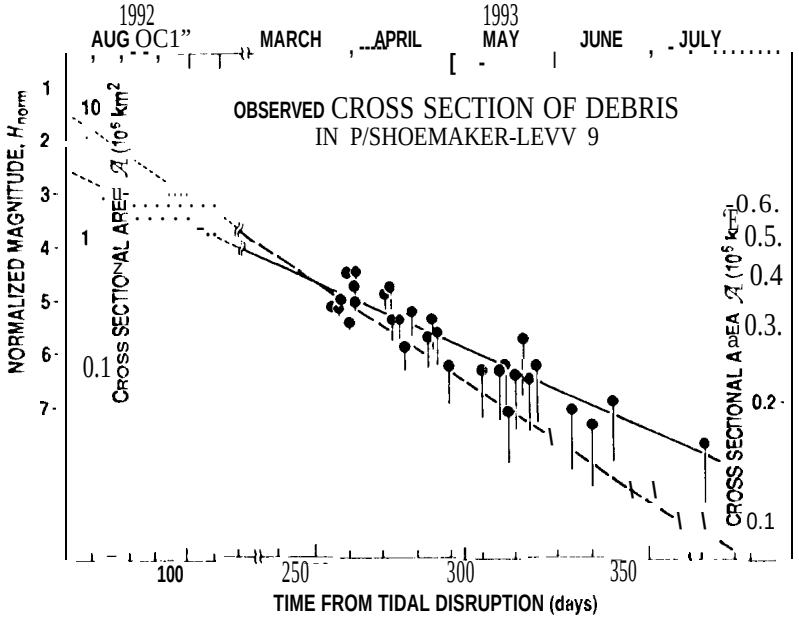

FIG. 4. Total visual brightness of 1'/Shoemakcr- Levy 9, normalized to 1 AU from both the Sun and Earth, and the cross-sectional area of its particulate debris vs. time from breakup. The dots are the data points reduced on the assumptions of a geometric albedo of 4% and a phase slope of 0.035 mag/deg. The lower ends of the bars arc the magnitudes when there is no phase effect. Extrapolations to the time of tidal disruption are from least squares solutions to the 30 data points.

The volume of space that was occupied by the debris at a time t shortly following the breakup is approximated by assuming an initially uniform isotropic expansion of the original volume of the nucleus. If the comet's equivalent pre-breakup nuclear radius was R_0 and the rate of expansion V_0, the volume $\mathcal{U}$ at t is simply given by:

$$\mathcal{U}(t) = \tfrac{4}{3}\pi \left[R_0 + V_0(t - t_0)\right]^3, \tag{17}$$

where t_0 indicates, as before, the time of splitting. A particle mean free path now becomes:

$$\ell(t) = \frac{477(.s2)}{3\mathcal{A}_0\left(s + (s)\right)}2 \left[R_0 + V_0(t - t_0)\right]^3. \tag{18}$$

Evidence points to a very low initial expansion velocity V_0, probably on the order of a few tenths of 1 In/s, in which case $V_0(t - t_0) << R_0$ for an hour or so after the breakup, depending on the size of the original nucleus. For a particle whose s $\simeq$ (s) $\simeq \langle s^2\rangle^{1/2}$, the initial mean free path is a function of R_0 and $\mathcal{A}_0$ only. This condition applies, for example, in the case of a size distribution of $^2 s^{-5} ds$ for particles whose dimensions are equal to a geometric mean of the distribution]'s largest and the smallest size. Even with R_0 as large as 5 km (Sec. 1), the mean free path amounts to less than 10 cm and each particle collides, on the average, ten times or so every second. For boulders and especially the large fragments the mean free path is many orders of magnitude smaller, which indicates that they must have been subjected to an intense (but low-velocity) bombardment by smaller debris. Later, when $V_0(t - t_0) >> R_0$, the mean free path would increase as $(t - t_0)^3$, but by then the various assumptions made—in particular that of a uniform isotropic expansion- may no longer hold even approximately. The mean free path can also be used to estimate the interval of time during which particle- particle collisions were important. Their total number, $\nu(t)$, experienced by a single grain between t_0 and t is

$$\nu(t) = \frac{R_0 V}{2\ell_0 V_0}\left\{1 - \left[1 + \frac{V_0}{R_0}(t - t_0)\right]^{-2}\right\}, \tag{19}$$

where $\ell_0 = \ell(t_0)$. From this expression it follows that- to the extent of its applicability- 50% of all collisions occurred during $t - t_0 \leq 0.4 R_0/V_0$, 75% during $t - t_0 \leq R_0/V_0$, and 90% during $t - t_0 \leq 2.2 R_0/V_0$, that is, on the order of 0,1 day or so. The total number of collisions that each particle underwent is estimated from (19) to be on the order of 10^5. It is thus certain that particle-particle collisions must have played a major role in the redistribution of the initial rotational velocities of the particulate debris. We now turn to the questions of what was the probable character of the collisions and what was their effect on the velocity field of the debris.

5. COLLISIONAL DISTRIBUTION OF PARTICLE VELOCITIES

Hartmann (1978) carried out laboratory experiments, in which he studied mechanics of low-velocity collisions, He dropped centimeter-sized projectiles of three different materials into flat rock targets and examined the critical impact velocities at which the projectiles began to fragment. The most intro esting results for cometary applications arc those

made with dirt clods, dry silicate particles resembling low-density aggregate grains, of which comet nuclei arc believed to be largely made. 'J'heir catastrophic disruption, which Hartmann defined by a ratio of $\mu \leq \frac{1}{2}$ between the mass of the largest fragment and the original mass, was observed by him to take place mostly at impact velocities of ~ 2 In/s, even though the scatter on the plot is considerable, showing data points with $\mu = 0.76$ at an impact velocity of 3.3 m/s and $\mu = 0.65$ at 4.7 in/s. Wc notice that these velocities are of the same order of magnitude as the orbits]-vc]oc.ity increment needed to explain the extent of the dust trails of P/Shoemaker-Levy 9. Hartmann also examined the degree of elasticity of the collisions, showing that even for high-density particles made of natural igneous rocks, the rebound velocities were generally only 25% to 60% of the impact velocities and much lower in the presence of any regolith.

To examine the collisional evolution of the])articlc-velocity distribution, we begin by considering an oblique collision between two spherical particles of masses m_1 and m_2. We introduce an inertial coordinate system, in which velocity vectors are referred to the center of mass of the parent comet. Since the impact vector (defined by the line of centers of the two particles and the contact point) is randomly oriented with respect to the pre-collision directions of motion of the particles, the axes of the coordinate system arc most conveniently chosen with the x-axis along the impact vector and the y- and z-axes in the tangential plane of the colliding particles. The degree of elasticity is expressed by the coefficient of restitution k, which decreases from unity for perfectly elastic collisions to zero for completely inelastic ones. Let the approach (pre-collision) velocity vectors of the two particles in this coordinate system be, respectively, $(\mathbf{V_1})_{\rm pre} = \{(\dot{x}_1)_{\rm pre}, (\dot{y}_1)_{\rm pre}, (\dot{z}_1)_{\rm pre}\}$ and $(\mathbf{V_2})_{\rm pre} = \{(\dot{x}_2)_{\rm pre}, (\dot{y}_2)_{\rm pre}, (\dot{z}_2)_{\rm pre}\}$ and similarly for the rebound (post-collision) velocity vectors, $(\mathbf{V_1})_{\rm post}$ and $(\mathbf{V_2})_{\rm post}$. Further, let $(V_1)_{\rm pre} = |(\mathbf{V_1})_{\rm pre}|$ and $(V_1)_{\rm post} = |(\mathbf{V_1})_{\rm post}|$, and similarly for particle 2. The rebou:)d-velocity components are related to the approach-velocity ones by (Osgood 1 949):

$$
\begin{aligned}
(\dot{x}_1)_{\rm post} &= \frac{(1 - k\mu_{21})(\dot{x}_1)_{\rm pre} + (1 + k)\mu_{21}(\dot{x}_2)_{\rm pre}}{1 + \mu_{21}}, \quad (\dot{y}_1)_{\rm post} = (\dot{y}_1)_{\rm pre}, \quad (\dot{z}_1)_{\rm post} = (\dot{z}_1)_{\rm pre}, \\
(\dot{x}_2)_{\rm post} &= \frac{(1 + k)(\dot{x}_1)_{\rm pre} + (\mu_{21} - k)(\dot{x}_2)_{\rm pre}}{1 + \mu_{21}}, \qquad (\dot{y}_2)_{\rm post} = (\dot{y}_2)_{\rm pre}, \quad (\dot{z}_2)_{\rm post} = (\dot{z}_2)_{\rm pre},
\end{aligned}
\tag{20}
$$

where $\mu_{21} = m_2/m_1$.

Collisional random-walk effects on the velocity field were modeled by applying a Monte Carlo approach. The test particle (particle 1) was '(launched" with a prescribed velocity $V_{\rm init} = (V_1)_{\rm pre}$ in a random direction, defined by an azimuth angle $(\alpha_1)_{\rm pre}$, which varied from 0 to 2π in the tangential plane and by an angle $(\beta_1)_{\rm pre}$, between O and π, which the velocity vector makes with the normal to the plane,

$$
\begin{pmatrix} (\dot{x}_1)_{\rm pre} \\ (\dot{y}_1)_{\rm pre} \\ (\dot{z}_1)_{\rm pre} \end{pmatrix} = V_{\rm init} \begin{pmatrix} \cos(\beta_1)_{\rm pre} \\ \cos(\alpha_1)_{\rm pre}\, \sin(\beta_1)_{\rm pre} \\ \sin(\alpha_1)_{\rm pre}\, \sin(\beta_1)_{\rm pre} \end{pmatrix}. \tag{21}
$$

For particle '2 one random number specified its relative mass μ_{21} and three more random numbers its pre-collision orbital velocity vector, $(V_2)_{\rm pre}$, $(\alpha_2)_{\rm pre}$, and $(\beta_2)_{\rm pre}$. From (20) we

then calculated $(\dot{x}_1)_{post}$ and determined $(V_1)_{post} = [(\dot{x}_1)^2_{post} + (\dot{y}_1)^2_{post} + (\dot{z}_1)^2_{post}]^{1/2}$. In the next step, this velocity was set equal to the approach velocity of the test particle for its collision with particle 3, all four parameters of which were defined by random numbers. However, in order to comply with the chaotic nature of oblique collisions and thus to justify the repeated application of the coordinate system tied to the impact vector and the tangential plane passing through the contact point, the two angles that characterize the direction of motion of the test particle upon its collision with particle 3 also had to be defined by random numbers. In this fashion, we subjected the test particle to $\sim 10^5$ collisions, consistent with the results of Sec. 4. Caution was exercised in applying a random number generator to any quantity whose rate of occurrence is value dependent. The reader is referred to Sekanina (1991) for an approach developed for the angles β_i (which have the highest occurrence rate at $\frac{1}{2}\pi$ and the lowest at O and π) and for the particle velocity distribution (which was assumed to yield an occurrence rate dropping exponentially with increasing velocity). Approximating the particle-mass distribution function by a power law, $h(m)\,dm \propto m^{-\chi}\,dm$ for $m_0 \leq m \leq m_\infty$ and h(m) = O for $m < m_0$ and $m > m_\infty$, the general approach yields for particle masses m_i $(i = 2,3, \ldots)$:

$$m_i = m_0 \left\{ 1 + \Re \left[\left(\frac{m_\infty}{m_0} \right)^{1-\chi} - 1 \right] \right\}^{\frac{1}{1-\chi}} = m_\infty \left\{ 1 + \Re' \left[\left(\frac{m_\infty}{m_0} \right)^{\chi-1} - 1 \right] \right\}^{\frac{1}{1-\chi}} \quad \text{if } \chi \neq 1,$$

$$= m_0 \left(\frac{m_\infty}{m_0} \right)^{\Re} = m_\infty \left(\frac{m_\infty}{m_0} \right)^{-\Re'} \quad \text{if } \chi = 1,$$

where $\Re$ is a random number from an interval (0, 1). The two alternative expressions given in either case reflect the obvious fact that any random number $\Re$ from the Unit interval can without detriment be replaced with $\Re' = 1 - \Re$.

From the formulation of the problem it is obvious that the results are model dependent. However, a characteristic feature of all our solutions was a rapid "thermalization" of the test particle, whose collisionally acquired mean velocity stabilized often after fewer than *5000* collisions and always after $\sim$*10000* collisions. Consequently, the particle's random walk also describes an *equilibrium collisional-velocity distribution* $\Psi(V_{eq})$ of the debris, In general terms, the dependence of the distribution's properties on the basic parameters for the assumed collisional scenarios can be summarized as follows:

(i) Initial particle velocity. Since the random walk of colliding particles was assumed to occur with velocities proportional to the initial velocity V_{init}, the results scale with it. We therefore present collisional distributions of dimensionless velocities expressed in units of the initial velocity, $\kappa = V_{eq}/V_{init}$. In many cases, the mean equilibrium velocity V_{eq} turned out to be appreciably higher than V_{init}, with a significant fraction of equilibrium velocities exceeding V_{init} by a considerable margin. The values of κ can thus effectively be perceived as collisions] enhancement factors.

(ii) Particle mass distribution. This affects the collisional-velocity distribution) in two ways. In terms of the power-]aw distribution assumed in *(22),* by far the most important factor is the mass index χ. The observed considerable extent of the dust trails can therefore be interpreted as duc to collisionally enhanced rotational velocities of the debris only if the particles involved have a relatively flat mass distribution $h(m)\,dm$, whose $\chi \simeq 1$. Much steeper distributions, whose $\chi >> 1$, were found to have virtually no effect on the velocities

of the debris, with the exception of particles with masses near m_0, the lower limit of the mass spectrum. Effects of the other mass-distribution parameter, the ratio m_∞/m_0, are far less significant.

(iii) Test particle's mass. As expected, effects of collisions on the velocity distribution were strongly particle-rna,ss dependent, the least massive particles having always been affected the most. An interesting result was obtained for the most massive fragments, whose equilibrium collisional velocities often tended to be *lower* than their initial velocities. The enhancement factors κ thus reflect in these cases a mitigation effect of the collisions, which may explain why the nuclear train is so much shorter than the trails.

(iv) Coefficient of restitution, The elasticity of particle- particle collisions also affects the velocity distribution, the equilibrium velocity increasing with increasing elasticity, Effects of the coefficient of restitution k on our Monte Carlo solutions appear to be particularly strong in the regime of highly elastic, collisions, which, however, were shown by Hartmann's (1 978) laboratory experiments to be unrealistic.

Table *3* lists distribution parameters for several of the hundreds of Monte Carlo runs carried out. All entries in the table refer to the ratio of $m_\infty/m_0 = 10^{22}$, but very similar results for the tabulated test particle masses were obtained with $m_\infty/m_0 = 10^{30}$. Since the expected mass of the brightest fragment is $m_\infty \simeq 10^{16}$ g at an assumed density of 0.'2 g/cm^3, the ratio $m_\infty/m_0 =$ *1022 implies* a lower particle-mass distribution cutoff at $m_0 \simeq 10^{-6}$ g. If of the above density, such grains would be $\sim$100 μm in radius and subjected to radiation-pressure accelerations of $\sim$3% of the solar attraction. The value of m_∞/m_0 adopted in the

TABLE 3. Monte Carlo solutions for the parameters of the collisional distribution of the velocity-enhancement factor κ (the adopted mass-range ratio $m_\infty/m_0 = 10^{22}$).

Mass inch, χ	Test particle's relative mass, $m_1/'mm$	Cocfficient of restitution, k	Distribution parameters of velocity-ell}larlcerrlcrlt factor κ						
			Mean value	Standard dcviation	Mode	Percentiles 50%	90%	95%	99%
1.0	$\leq 10^{-15}$	*0.0*	1.6	±1.1	0.9	1.4	3.1	3.8	5.5
		0.4	2.5	±1.6	1.5	2.1	4.6	5.6	8.0
	10^{-5}	0.0	1.5	±1.0	0.9	1.3	2.9	3.6	5.2
		0.4	2.3	±1.5	1.2	1.9	4.2	5.2	7.6
	0.01	0.0	1.3	±0.9	0.8	1.1	2.5	3.1	4.6
		0.4	1.9	41.4	1.0	1.6	3.6	4.5	6.8
	1	0.0	0.7	±0.4	0.5	0.6	1.2	1.5	2.1
		0.4	*0.8*	±0.5	0.6	0.7	1.5	1.9	2.7
1.2	$\leq 10^{-15}$	0.0	1.4	±0.9	0.8	1.1	2.6	3.2	4.7
		0.4	1.9	±1.4	1.3	1.6	3.6	4.5	7.1
	10^{-5}	*0.0*	1.4	±1.0	0.8	1.2	2.8	3.4	4.3
		0.4	1.9	±1.2	1.0	1.5	3.6	4.3	5.7
	1	0.0	0.8	40.1	0.8	0.8	1.1	1.1	1.2
		0.4	1.0	±0.1	0.9	0.9	1.2	1.3	1.4
1.4	$\leq 10^{-15}$	0.0	1.1	±0.7	0.7	0.9	2.0	2.5	3.6
		0.4	1.3	±0.9	0.7	1.1	2.4	3.4	4.7
	10^{-5}	{0.0 0.4}	1.0	±0.0	0.9	0.9	1.1	1.1	1.1
	1	{0.0 0.4}	1.0	±0.0	0.9	0.9	1.0	1.1	1.1

table approximates a combined particle-mass range in the train, the trails, and the bright portion of the tail region (See,. 8). On the other hand, the mass ratio of $m_\infty/m_0 = 1030$ implies a lower cutoff at $m_0 \simeq 10^{-14}$ g, referring to submicron-sized particles.

The first three columns of 'J'able 3 list selected values of the remaining parameters-~ the mass index, the test particle's mass, and the restitution coefficient, each of which affects the en h ancement factors κ in a profound manner. Not included arc the results from runs for the mass indices $\chi <$ I (very flat particle-mass distributions) and for $\chi >$1.4, which confirmed the general trend that is apparent from the table. Wc noted, however, that the parametric values for the equilibrium velocity distribution) were rather insensitive to the mass index outside the tabulated range, in that virtually no collisional effects were apparent for $\chi >$1.4 and that the results for $\chi <$ I almost coincided with those for $\chi = 1$. Als o omitted from Table 3 is information] from runs carried out for additional test-particle masses 7 - 1 2$_1$. The least massive particles tabulated have $m_1 \simeq 10$ g and an equivalent diameter of about 5 cm. Such pebbles could not be subjected to radiation-pressure accelerations greater than ~0.01% of the solar attraction and in March- July 1993 they sh ould have been situated within *0.5* arcsec of the calculated locus for objects with purely gravitational orbits. Interestingly, solutions for particles much less massive than 10 g yielded essentially the same results, which suggests that the equilibrium velocity distributions in the dust trails and the bright portion of the tail region arc alike. As far as the elasticity effects arc concerned, the tabulated results were restricted to two values of the restitution coefficient, $k =$ O and $k =$ 0.4, which presumably bracket the most probable scenarios. Solutions for unrealistic, more elastic collisions implied much higher velocities.

The last seven columns of Table 3 provide information 011 the equilibrium distributions of the enhancement factors κ. To describe the strongly non-Gaussian distributions as completely as possible, listed among the parameters arc, besides the mean value and the standard deviation, the mode and four percentiles, including a median. Their inspection reveals a number of characteristic features and systematic trends. Perhaps the most significant trait is a long tail toward very large values of κ for all particle masses except near the upper limit of the mass spectrum. The strong nonlinearity of this effect with particle mass is apparent from comparisons in 'J'able 3 of the characteristic values of κ, such as the mean or the median. For example, for $\chi = 1$ ant] $k =$ O, the mean value of κ decreases by only 0,1 over 10 orders of magnitude in mass, from $10^{-15} m_\infty$ to $10^{-5} m_\infty$, by 0.2 over the next three orders of magnitude, but by fully 0.6 over the mass range from 0.01 m_∞ to m_∞. In reality, the discrimination]] between the very massive fragments and other particles is even more dramatic than appears from these comparisons. The small number of very massive fragments implies that there are no objects in the distribution's upper percentiles and suggests, consequently, that collisions typically result in a decrease in the equilibrium velocity of these objects ($\kappa <$ I).

The broad range of collisions] velocity-enh ancement effects is illustrated in Fig. 5, which displays four steady-state distributions of κ. For our modeling needs (Sec. 6) the correlation with the test particle's mass is of primary interest. When $\chi \simeq 1$, a velocity enhancement by a factor of ~4 or more is attained by fully 5-] 5% of particles with masses of ~1 O g and by a factor of ~5–6 or more by 1 --5% of them. Thus, κ near 6 is apparently representative of the dust near the trail endpoints. On the other hand, the characteristic κ value for the fragments near the upper limit of the mass spectrum is close to the distribution's median because of their very limited number. This value could be as low as 0.6 for $\chi \simeq 1$.

6. MODELING THE DEBRIS EVOLUTION FOR A TIDALLY DISRUPTED ROTATING COMET

We are now ready to formulate a model for the evolution of P/Shoemaker-Levy 9's debris. Having reproduced Scotti and Melosh's (1993) results, we verified that some dispersion of the debris in both the nuclear train and the dust trails could be effected by Jupiter's radial differential perturbations. Applying a rigorous approach, we showed in Sec. 3 that the debris could also be dispersed in space as a result of slight differences among particle velocities in the direction of the comet's orbital motion. Developing a Monte Carlo collisional model, we established in Sees. 4 and 5 that such a velocity dispersion can be produced by particle–particle collisions in the cloud of debris subsequent to the tidal disruption of the progenitor nucleus. In particular, we ascertained that there was a tendency for the collisions to increase the velocities of particles that populate the dust trails, but to mitigate the motions of the very massive fragments that line up along the nuclear train. On the other hand, effects of gravitational interaction in the cloud of debris were found to be relatively unimportant,

Let us assume that at the time of tidal disruption a piece of debris on the spinning nucleus had the component of its rotational velocity in the direction of the cornet's orbital motion equal to V_{rot}. Let us also assume that the initial distribution of rotational velocities

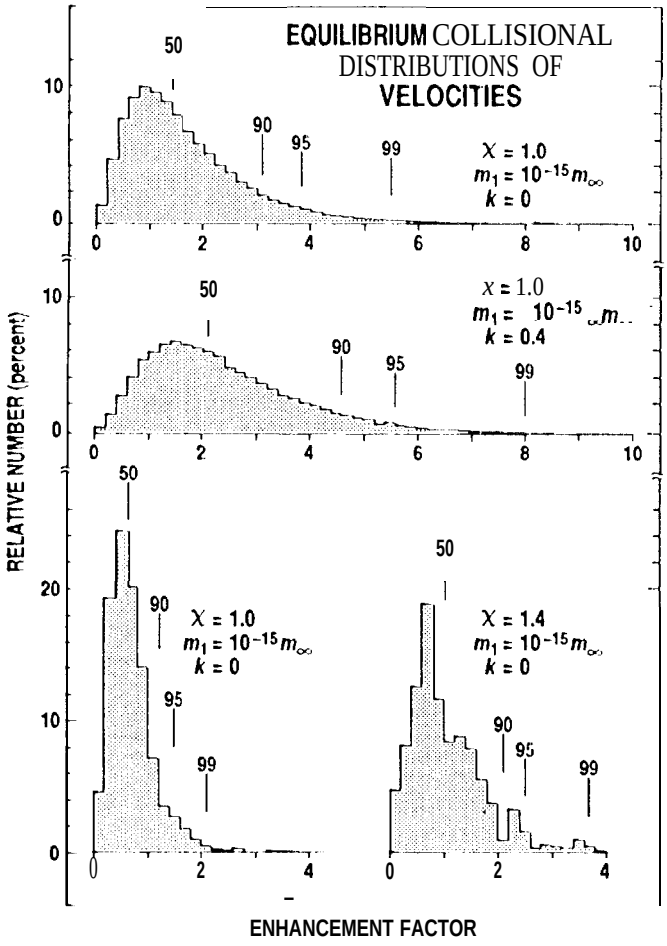

FIG. 5. Examples of the velocity-enhancement distribution calculated as a function of the collisional parameters: the mass index χ; the particle mass m_1, in units of the upper limit of the mass spectrum, m_∞; and the coefficient of restitution, k. Plotted on the abscissa is the dimensionless velocity-enhancement factor, κ, defined as the ratio of a particle's equilibrium collisional velocity to its initial velocity. All four distributions assume the mass range ratio of $m_\infty/m_0 = 10^{22}$, where m_0 is the lower limit of the mass spectrum. Identified are the 50, 90, 95, and 99 percentiles of each distribution

in the cloud of debris was the sole source for the velocity dispersion. We therefore identify the particle rotational velocity component V_{rot} with the velocity V_{init} (Sec. 5) and the observed impulse ΔV_{orb} (Sec. 3) with the collisionally acquired equilibrium velocity V_{eq} (Sec. 5). If the particle's enhancement factor is κ, we have:

$$\Delta V_{orb} = \kappa V_{rot} . \qquad (23)$$

Since the collisional redistribution of the ~)ar tic]c-velocity field is a stochastic process, the particles with the highest initial velocities V_{rot} are the most likely ones to end up with the highest velocities ΔV_{orb}. As our aim is to explain the lengths of the nuclear train and the dust trails, our primary interest is to find appropriate upper limits to ΔV_{orb}. For the less massive debris (boulders, pebbles, grains), the peak velocities are statistically most likely to have been acquired by particles on the surface of the original nucleus. Since a different argument applies to kilometer-sized chunks, the conditions for ΔV_{orb} are in the following treated separately for the trail debris and the fragments in the train.

Let a comet's s})i]l-vector orientation relative to the osculating jovicentric orbit at the time of tidal breakup, *to,* be given by the obliquity I and the argument Φ of the subjovian meridian at perijove. Let P be an arbitrary point on the nuclear surface, whose unit position vector relative to the center of mass at the time t_0 is $\mathbf{U}\{\theta, \phi\}$, where O is the point's angular distance from the subjovian meridian at that time and ϕ is its angular distance from the comet's equatorial plane, and let $R(\theta, \phi)$ be its distance from the center of mass or the local nuclear radius (Fig. 6). The components of U in the direction away from Jupiter, U_R, in the direction perpendicular to U_R and ahead of the comet in its orbital plane, U_T, and in the direction of the northern orbital pole from which the comet is seen to orbit Jupiter counterclockwise, U_N, can be expressed by (Sekanina 1981):

$$\begin{pmatrix} U_R \\ U_T \\ U_N \end{pmatrix} = - \begin{pmatrix} \cos(\Phi + u_0) \cos I & \sin(\Phi + u_0) & \sin I \sin(\Phi + u_0) \\ -\sin(\Phi + u_0) \cos I & \cos(\Phi + u_0) & \sin I \cos(\Phi + u_0) \\ 0 & \sin I & -\cos 1 \end{pmatrix} \begin{pmatrix} \cos\phi \cos(\theta + \theta_0) \\ \cos \phi \sin(\theta + \theta_0) \\ \sin \phi \end{pmatrix}, \quad (24)$$

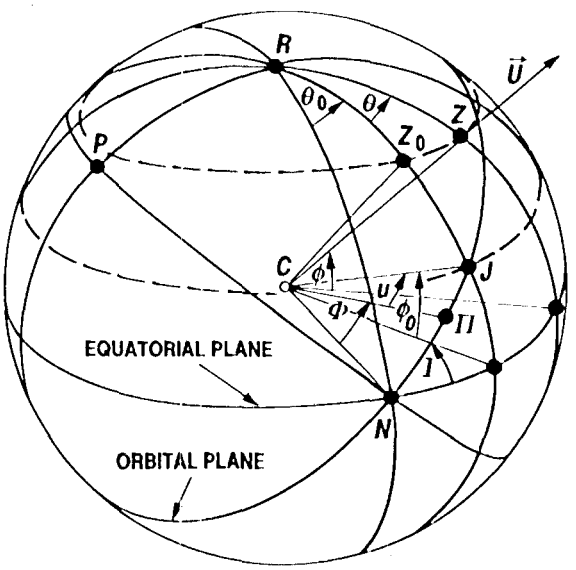

FIG. 6. orientation on a comet's rot ating nucleus. C is its center, P the northern pole of the comet's jovicentric orbit, R the northern pole of rotation, h' the comet's vernal equinox, and 1[the subjovian point at perijove. Angle I is the obliquity of the orbital plane to the equatorial plane and angle Φ is the argument of the subjovian meridian at perijove. At some time t, the subjovian point is at J, so that u is then the true anomaly, θ_0 the longitude of the subjovian point from the vernal equinox, and ϕ_0 its latitude. The location of a particle on the surface, at latitude ϕ, is shown by point Z_0 when it transits across the subjovian meridian and by Z a little later, when its meridian angle is θ and its longitude from the vernal equinox, $\theta + \theta_0$. U is a unit vector passing through point Z and directed radially away from the nucleus center.

where u_0 is the comet's true anomaly in the jovicentric orbit at the time t_0 and θ_0 is the cometocentric longitude of the subjovian meridian from the orbital plane's ascending node on the equatorial plane, whit.1] is equal to:

$$\tan \theta_0 = \cos I \tan(\Phi + u_0). \tag{25}$$

The quadrant of 0_0 is that of $\Phi + u_0$ when $I < 90°$ and that of $360° - (\Phi + u_0)$ when $1 > 90°$.

The difference in the radial distance, $\Delta r(\theta, \phi)$, between the point P and the comet's center of mass at the time t_0 (Sec. 3) is obviously:

$$\Delta r(\theta, \phi) = R(\theta, \phi)\, U_R(\theta, \phi), \tag{26}$$

which yields the quantity $(\Delta r)_{dust}$ for determining Jupiter's radial differential perturbations of the debris.

Even though gravitational perturbations among the individual pieces of the debris were shown in Sec. 4 to be relatively unimportant, they Were likely to affect the equilibrium ~)articlc-velocity distribution] to some extent. The peak rotation velocity was certainly lower than the surface escape velocity from the progenitor nucleus. Upon breakup, not only were velocities of some particles increased WC]] beyond the escape velocity from the parent comet, but as the fragmentation progressed and the cloud of material expanded, it became much easier to escape from the gravitational field of any fragment. However, the observed impulse ΔV_{orb} for the nuclear train is also lower than the probable escape velocity from the parent comet and it is conceivable that neglect of a gravitational interaction among particles could lead to an overestimate of the equilibrium collisional velocities, especially for the most massive fragments. Considering the absence of information on the details of the tidal-disruption process, we doubt that the magnitude of this effect could be derived rigorously. We point out, however, that the resulting velocity correction due to gravitational interaction, δV, can formally be accounted for by rewriting (23) for the trail debris, $(\Delta V_{orb})_{dust}$, and for the kilolnctcr-sized fragments, $(\Delta V_{orb})_{nucl}$, as follows:

$$\begin{aligned} (\Delta V_{orb})_{dust} &= \kappa_{dust}(V_{rot})_{dust} - \delta V = \kappa^*_{dust}(V_{rot})_{dust}, \\ (\Delta V_{orb})_{nucl} &= \kappa_{nucl}(V_{rot})_{nucl} - \delta V = \kappa^*_{nucl}(V_{rot})_{nucl}, \end{aligned} \tag{27}$$

where we adopt, following our results in Sec. 5 and the above arguments, $\kappa^*_{dust} \approx \kappa_{dust} \approx 6$ for particles at the outer ends of the dust trails and $\kappa^*_{nucl} \approx 0{,}5 < \kappa_{nucl}$ for the large fragments in the nuclear train.

If P_{rot} is the rotation period at the time of tidal disruption, the relevant components ω_R, ω_T, and ω_N of the cornet's spin vector $\boldsymbol{\omega}$ in the jovicentric coordinate system arc at to:

$$\begin{pmatrix} \omega_R \\ \omega_T \\ \omega_N \end{pmatrix} = \frac{2\pi}{P_{rot}} \begin{pmatrix} -\sin I \sin(\Phi + u_0) \\ -\sin I \cos(\Phi + u_0) \\ \cos I \end{pmatrix}. \tag{28}$$

Since the rotation-velocity vector is equal to $\mathbf{V}_{rot} = R(\boldsymbol{\omega} \times \mathrm{U})$, the radial and transverse velocity components of the debris at a point P arc in the RTN jovicentric-oriented coordinate system at the time t_0:

$$(V_{\rm rot})_{\rm R} = -\frac{2\pi}{P_{\rm rot}} R(\theta,\phi)\left[U_{\rm T}(\theta,\phi)\cos I + U_{\rm N}(\theta,\phi)\sin I\cos(\Phi+u_0)\right],$$
$$(V_{\rm rot})_{\rm T} = +\frac{2\pi}{P_{\rm rot}} R(\theta,\phi)\left[U_{\rm R}(\theta,\phi)\cos I + U_{\rm N}(\theta,\phi)\sin I\sin(\Phi+u_0)\right]. \qquad (29)$$

The relevant contribution from $\mathbf{V}_{\rm rot}$ in the direction of the comet's orbital-velocity vector, $(V_{\rm rot})_{\rm dust}$, is given by the dot product $\mathbf{n}\cdot\mathbf{V}_{\rm rot}$, where n is a unit orbits]-velocity vector in the RTN coordinate system at the time of breakup. The expression is greatly simplified, if the comet's orbital arc of interest, in the immediate proximity of the perijove, is approximated by a parabola. Then $\mathbf{n} = \{\sin\frac{1}{2}u_0, \cos\frac{1}{2}u_0, 0\}$ and

$$(V_{\rm rot})_{\rm dust} = \frac{2\pi}{P_{\rm rot}} R(\theta,\phi)\left[(U_{\rm R}\cos\tfrac{1}{2}u_0 - U_{\rm T}\sin\tfrac{1}{2}u_0)\cos I + U_{\rm N}\sin I\sin(\Phi+\tfrac{1}{2}u_0)\right]. \qquad (30)$$

Since the preferred mode of tidal disruption is along planes perpendicular to the radial direction from the perturbing planet (e.g., Aggarwal and Oberbeck 1974, Dobrovolskis 1990), the probable shape of the large fragments that populate the nuclear train will tend to be slice-like, the boundary planes of each fragment being approximately perpendicular to the radial direction. The position of a fragment's center of mass is described as a mean value of the positions of all points $P\{R,\theta,\phi\}$ on the surface of the disintegrating original nucleus that have the same radial distance from Jupiter and whose angular coordinates satisfy a condition of $\sin\phi = c_1 + c_2\cos\phi\sin(\theta+c_3)$, where c_1, c_2, and c_3 depend on the rotation constants I and Φ. The initial RTN coordinates of the fragment's center of mass relative to the center of mass of the progenitor nucleus are $\{R(\theta,\phi)U_{\rm R}(\theta,\phi), {\rm O}, {\rm O}\}$, so that the quantity $(\Delta r)_{\rm nucl}$, which determines the jovian radial differential perturbations on the massive fragments in the train, is given by the same expression (26) as that for the *other* debris, $(\Delta r)_{\rm dust}$. The radial component of the rotation velocity of the fragment's center of mass is always zero and the velocity's contribution in the direction of the orbital-velocity vector, $(V_{\rm rot})_{\rm nucl}$, derives entirely from its transverse component:

$$(V_{\rm rot})_{\rm nucl} = \frac{2\pi}{P_{\rm rot}} R(\theta,\phi)U_{\rm R}(\theta,\phi)\,{\rm Cos}\,I\,{\rm Cos}\,\tfrac{1}{2}u_0. \qquad (31)$$

The projected lengths of the nuclear train, $\Lambda_{\rm nucl}$, and the two dust trails, $\Lambda^{\rm ene}_{\rm dust}$ and $\Lambda^{\rm wsw}_{\rm dust}$, measured from the train's middle in, say, arcsec, yield the following conditions for the effects due to the jovian radial differential perturbations and the velocity increment:

$$\begin{aligned}
&\max_{\{\theta,\phi\}}\left[a\,(\Delta r)_{\rm nucl} + b\,(\Delta V_{\rm orb})_{\rm nucl}\right] = \tfrac{1}{2}\Lambda_{\rm nucl},\\
&\max_{\{\theta,\phi\}}\left[a(\Delta r)_{\rm dust} + b\,(\Delta V_{\rm orb})_{\rm dust}\right] = \Lambda^{\rm ene}_{\rm dust},\\
&\max_{\{\theta,\phi\}}\left[a(\Delta r)_{\rm dust} + b\,(\Delta V_{\rm orb})_{\rm dust}\right] = \Lambda^{\rm wsw}_{\rm dust},
\end{aligned} \qquad (32)$$

where a (in arcsec per km) and b (in arcsec per m/s) are the rates of the two dispersion effects, which vary with both the time of observation and the time of tidal disruption. We note that they are related to the coefficients A and B from (4):

$$a = \frac{B}{2A}\Lambda_{\rm nucl} = \frac{0.56}{z^2}\Lambda_{\rm nucl},$$
$$b = \frac{1}{2A}\Lambda_{\rm nucl} = \frac{2.67}{\sqrt{z}}\Lambda_{\rm nucl}. \qquad (33)$$

The symbol $\max_{\{\theta,\phi\}}$ for a given spin-vector orientation in (32) indicates the peak values attained by the bracketed expressions over the entire nuclear surface, that is, among all possible combinations of $\{0, \phi\}$. These maxima determine the observed extents of the nuclear train and the dust trails that enter the right-hand sides of (32). The values of θ and ϕ for which the maxima are reached are generally different for the train and the trails, Since the bracketed expressions are symmetrical with respect to the comet's center of mass and since the expressions on the left-hand sides of the second and the third lines are identical, the condition $\Lambda_{\rm dust}^{\rm ene} < \Lambda_{\rm dust}^{\rm wsw}$ from Table 2 implies nonsphericity of the parent nucleus and/or different properties of particles that populate the two trails. In any case, one can introduce an effective radius of the original nucleus, $R_{\rm eff}$, and combine the first condition of (32) with the second or the third one to find, after incorporating (33):

$$f(I, \Phi; P_{\rm rot}; \kappa_{\rm nucl}^*)R_{\rm eff} = A,$$
$$g(I, \Phi; P_{\rm rot}; \kappa_{\rm dust}^*)R_{\rm eff} = A\lambda, \qquad (34)$$

where $\lambda = 2\Lambda_{\rm dust}^{\rm ene}/\Lambda_{\rm nucl}$ or $2\Lambda_{\rm dust}^{\rm wsw}/\Lambda_{\rm nucl}$ and

$$f(I, \Phi; P_{\rm rot}; \kappa_{\rm nucl}^*) = \max_{\{\theta,\phi\}}\left[U_{\rm R}\left(B + \frac{2\pi}{P_{\rm rot}}10^3\kappa_{\rm nucl}^*\cos I\cos\tfrac{1}{2}u_0\right)\right],$$
$$g(I, \Phi; P_{\rm rot}; \kappa_{\rm dust}^*) = \max_{\{\theta,\phi\}}\left[U_{\rm R}B + \frac{2\pi}{P_{\rm rot}}10^3\kappa_{\rm dust}^*\left\{(U_{\rm R}\cos\tfrac{1}{2}u_0 - U_{\rm T}\sin\tfrac{1}{2}u_0)\cos I + U_{\rm N}\sin I\sin(\Phi + \tfrac{1}{2}u_0)\right\}\right], \qquad (35)$$

with $P_{\rm rot}$ in s and the factors 103 introduced in order to adjust the units of the velocity terms from s^{-1} to $m\ s^{-1}\ km^{-1}$ to conform with the units of the coefficient B.

The equations (34) represent two independent conditions for $R_{\rm eff}$, both of which must be satisfied at the same time, if the lengths of the nuclear train and the dust trails are to be interpreted as manifestations of the same disruption event and the associated post-breakup phenomena. Before we present the numerical results, we point out that $U_{\rm R}$ is the only quantity in the first equation of (35) that depends on θ and ϕ. Since $\max_{\{\theta,\phi\}}[U_{\rm R}(\theta,\phi)] = 1$ and $2 = \sec^2\frac{1}{2}u_0$, the first equation of (34) can be written in terms of z, thus indicating a symmetry of the solutions with respect to perijove:

$$R_{\rm eff} = \frac{0.89z^2}{1 + 1.13\left(\dfrac{P_{\rm crit}}{P_{\rm rot}}\right)z\,\kappa_{\rm nucl}^*\cos I}, \qquad (36)$$

where $P_{\rm crit}$ is the critical rotation period at an assumed nuclear density of 0.2 g/cm^3 and equal to 7.38 hr or 0.3075 day [cf. the text that follows Eq. (5) in Sec. 3]. The units

of P_{crit} and $P_{rot} \geq P_{crit}$ arc the same, while R_{eff} is again in km. The constraints on the relationship between the rotation period and the obliquity arc set by the second equation of (34), so that Eq. (36) is not by any means valid for all values of P_{rot} and I. We point out that when the time of tidal disruption is assumed to coincide with the time of perijove ($z = 1$) and when the obliquity is assumed to reach 90°, the relation (36) yields a size of the progenitor nucleus that is almost identical with the size derived by Scotti and Melosh (1 993). However, we will show below that because of the constraints set by the trail length on the function $g(I, \Phi; P_{rot}; \kappa^*_{dust})$, this result cannot be defended in the framework of our cone.cptual model.

7. ADDITIONAL EVIDENCE FROM THE BRIGHT FRAGMENTS

One of the results of the comet's imaging with the Hubble Space Telescope (HST) on July 1, 1993 was, according to Weaver *et al.* (] 993), a discrimination of the brightest fragment- a single, somewhat elongated feature when observed with large ground-based instruments--into at least four components. The two main components appear on Weaver *et al.*'s Fig. 2 to be ~0.3 arcsec apart, along a position angle of ~1 20°–3000, that is, in a direction that makes an angle of 40°---500 with the nuclear train.

Because of this peculiar orientation of the pair, wc suspect that the two components could be products of a more recent breakup. While it is impossible to determine the time and circumstances of this presumed secondary splitting, we searched for scenarios consistent with the pair's separation distance and position angle on the HST image, neglecting effects of the gravitational interaction between the components. We found a large number of solutions involving very low separation velocities, selected examples of which arc listed in Table 4. We also found less attractive solutions based solely on Jupiter's radial differential perturbations and suggesting breakup times closer to perijove. '1'here is a precedent for the kind of secondary breakup suggested by the scenarios in Table 4. A satisfactory solution to the orbital motion of one of the companions to the principal component of Periodic Comet Brooks 2, observed in] 889 following the comet's close approach to Jupiter in 1 886, could only be derived on the assumption] that this companion broke away from the other companion approximately 1 $\frac{1}{2}$ years after the splitting of the progenitor nucleus at Jupiter (Sekanina 1977).

TABLE 4. Examples of solutions consistent with a separation distance of 0.3 arcsec at a position angle of 300° between the two main components of the brightest fragment of P/Shoemaker–Levy 9.

Assumed time of the pair's splitting (0^hTDB)	Time elapsed from perijove (days)	Distance from Jupiter (AU)	Separation velocity of the nucleus pair (m/s)			
			No normal component		No cross-track component	
			Orbital-velocity component	Transverse component	Orbital-velocity component	Normal component
1992 July 10	2	0.0162	+ 0.005	-0.)2	+0.006	+0.17
15	7	0.0380	+ 0.007	-0.08	+0.010	+0.12
Aug. 1	24	0.0849	+0.012	-0.06	+0.016	+0.09
Sept. 1	55	0.1420	40.016	--0.05	4-0.023	-10.08
Nov. 1	116	0.2175	40.024	-0.06	-10.036	+0.08
1993 Jan. 1	17i'	0.2681	40.030	–0.08	+0.054	-10.10

Because of the role of the mass distribution function, $h(m)\,dm$, in the steady-state particle-velocity distribution, we checked whether the mass law implied by the collisional model developed in *Sm.. 5* is consistent with Weaver *et al.*'s (1993) sequence of photometrically determined dimensions of the 11 brightest fragments, assuming the same bulk density. Writing $h(m)\,dm = (h_0/m)\,dm$, where h_0 is a constant, the number of fragments whose masses are equal to or exceed m is

$$n(m) = \int_m^{m_\infty} h(m)\,dm = h_\infty - h_0 \ln\left(\frac{m}{m_{\rm norm}}\right), \tag{37}$$

where m_∞ is again the upper limit of the particle mass distribution, $m_{\rm norm}$ is an arbitrary normalization mass, and $h_\infty = h_0 \ln(m_\infty/m_{\rm norm})$. The progenitor comet's mass, calculated as a sum of the masses of all fragments, is then

$$M = \int_{m_0}^{m_\infty} m\,h(m)\,dm = h_0(m_\infty - m_0) \doteq h_0 m_\infty, \tag{38}$$

where $m_0 << m_\infty$ is again the lower limit of h(m) and the mass of the debris is dominated by the contributions from the largest fragments. Combining (37) with (38), we find

$$M = h_0\, m_{\rm norm} \exp\left(\frac{h_\infty}{h_0}\right). \tag{39}$$

Applying (37) to Weaver *et al.*'s (1 993) sequence of 11 fragments, whose photometrically determined sizes were converted into masses assuming a bulk density of 0.'2 g/cm^3, we obtained an excellent agreement when the faintest piece was ignored, with the result

$$\begin{aligned} h_0 &= +\,7.434 \pm 0.21, \\ h_\infty &= -0.40 \pm 0.20, \end{aligned} \tag{40}$$

with the masses expressed in units of 10^{16} g. When the 11th fragment was included, the two parameters became $h_0 = +6.57 \pm 0.45$ and $h_\infty = +0.16 \pm 0.49$, also yielding an acceptable solution. From (39) and (40) we found $M = 10^{16.85 \pm 0.02}$ g and, converting the nuclear mass back into the radius (thus eliminating any effects of the assumed density), we obtained for the progenitor $R_{\rm eff} = 4.4 \pm 0.1$ km. The formal error, although not quantitatively meaningful, indicates a high degree of correspondence between theory and observation. The other set of parameters ho and h_∞ yielded a radius that was smaller by only 0.1 km, '1'bus, we not only confirmed that the assumed m^{-1} law is consistent with the size distribution of the largest fragments, but we were also able to derive an estimate for the radius of the progenitor nucleus. In addition, extrapolating (37) to $n = 2$], we found a mass of $\sim 10^{14.75}$ g and an effective radius of nearly 0.9 km for the faintest of the 21 fragments.

8. APPL1[CATION OF THE RO'I'ATION MODEL AND CONCLUSIONS

Because of the multitude of parameters that enter Eqs. (34), the conditions for $R_{\rm eff}$ were expected to be satisfied by a large number of solutions, which we tried to constrain as much as possible. Based on the results of Sees. 5 and 6, the enhancement factors for the nuclear

train and the dust trails were in most runs assumed to be $\kappa^*_{\rm nucl} = 0.5$ and $\kappa^*_{\rm dust} = 6$. These values reflect our preference for the model with $\chi \simeq 1$ of the mass distribution function of the debris involved [cf. (22)]. Support for this law was demonstrated in Sec. 7. Effects of varying $\kappa^*_{\rm nucl}$ and $\kappa^*_{\rm dust}$ on the solutions are briefly addressed below.

One of the two remaining fundamental parameters, the effective time of disruption t_0, was calculated from high-quality data of the nuclear train's orientation, as described later in this section, while the other, the trail-to-train length ratio λ, was found from available wide-field imaging. Since the dust trails are features of a low surface brightness, fading gradually away with increasing distance from the nuclear train, their detected extent, depends on the observing circumstances, the exposure time in particular. The model's most severe test is offered by λ derived from the maximum length estimate for the more extended, west-southwestern trail. From Table 2, $(\Lambda^{\rm wsw}_{\rm dust})_{\rm max} \simeq 10.5$ arcmin at a time when the length of the nuclear train was $\Lambda_{\rm nucl} = 51$ arcsec (Scotti and Melosh 1993), yielding $\lambda \simeq 25$. The length of the shorter, cast-northeastern trail, whose $(\Lambda^{\rm ene}_{\rm dust})_{\rm max} \simeq 6.2$ arcmin in I'able 2, implies, very crudely, $\lambda \simeq 15$ ant] could contain debris from a host of locations in the original nucleus that satisfy the second condition of (32). One of the solutions is obtained by maximizing the bracketed expression, that is, by applying the same quantity $g(I, \Phi; P_{\rm rot}; \kappa^*_{\rm dust})$ that was derived for the west-sout]lwestcrll trail, in which case $|(\Delta r)_{\rm dust} \leq (\Lambda^{\rm ene}_{\rm dust} / \Lambda^{\rm wsw}_{\rm dust}) R_{\rm eff}$ for the east-northeastern trail. A multitude of solutions can similarly be offered for any interior point along either of the two trail branches.

As discussed below, an assumption that the tidal breakup of the progenitor occurred at any particular instant is artificial, because the episode must have been characterized by a finite duration. However, modeling of the debris evolution should take into account the fact that the highly organized forces involved, such as the jovian radial differential perturbations, are rather inefficient during the early phase when particle motions are chaotic due to intense collisional interaction. As a result, the *effective* time of breakup that enters the expressions for the evolution of the debris should follow the period of physical disruption of the parent, comet with a lag that is characteristic of the tin-m spanned by intense collisions, whit]), as established in Sec. 5, was crudely *O.]* day. On the other hand, of course, it is plausible that the tidal breakup began *before* perijove, which leaves us with no clear guidance as to what was the effective time of breakup t_0, to be employed in the equations, relative to perijove.

We began our investigation of solutions to the conditions (34) by examining the case of the effective time of breakup coinciding with perijove. The first of the two conditions was used in its form (36), while the evaluation of the coefficients $g(I, \Phi; P_{\rm rot}; \kappa^*_{\rm dust})$ was conducted in a three-dirnel]sional phase space, in which the obliquity I was varied from 0° to 180° and the argument Φ from 0° to 360°, both at steps of 10°, whereas the period $P_{\rm rot}$ was varied from $P_{\rm crit} = 7.38$ hr to several days at progressively increased steps. It soon became obvious that for a slowly rotating nucleus, $P_{\rm rot} >> P_{\rm crit}$, the contributions of the velocity terms in *(35)* and (36) became so small that they had hardly any effect on the solutions, in that the nuclear radius calculated as $A\lambda/g$ always turned out to be much larger than that calculated as A/f. Although the difference between the values of $R_{\rm eff}$ derived from the two conditions decreased with decreasing $P_{\rm rot}$ as well as with I approaching 180°, for no combination of I, Φ, and $P_{\rm rot}$ were they found to coincide. We concluded that, within the constraints of our conceptual model, *the* assumption of a *tidal* disruption *at perijove yielded no solutions.*

The next step was to investigate solutions for various other assumed times of breakup. Two examples, displayed in Fig. 7, illustrate a symmetry with respect to perijove. The leaf-shaped areas of solutions are bounded by the critical period at the bottom and terminate in a tip at $I = 180°$ on the right. Two curved boundaries connect the base at P_{crit} with the tip: the upper curve, calibrated in Fig. 7 with the values of the nuclear radius R_{eff} increasing from the left to the right, is characterized by a constant argument of subjovian meridian which is equal to $\Phi = 900 - \frac{1}{2}u_0$ or $270° - \frac{1}{2}u_0$ and shows that the minimum nuclear radius that satisfies both conditions (34) corresponds to the critical rotation period and to the lowest obliquity. The lower curve is an isoline of the maximum nuclear radius that satisfies the two conditions. The curves that connect the upper curve. with the base $P_{rot} = P_{crit}$ and lie in between the two boundaries were calculated from (36) and represent the isolines for some intermediate values of the nuclear radius. Each solution between the two boundary curves is satisfied for four different values of Φ, whit.11 for $P_{rot} = \text{const.}$ closely satisfy a condition of the type:

$$\Phi =] 80° \cdot j - \frac{1}{2}\left[u_0 \pm \arccos(w_1 + w_2 \cos I)\right], \tag{41}$$

where w_1 and w_2 are coefficients that depend on the parameters of the solutions, such as the rotation period and the time of disruption, and j stands for any of the four possible values, $j = -1, 0, +1, +2$, such that Φ is in the interval of (0°, *3600).* For example, for $P_{rot} = 7.38$ hr and $t_0 = T_J + 0.1$ day we found $w_1 = -0.82198$ and $w_2 = -4.36018$, with the adopted values for κ^*_{nucl}, κ^*_{dust}, and λ. A limiting condition of $\cos I = -(1 + w_1)/w_2$ yields $I = \mathbf{87".7}$ and, with $j = +1$, $\Phi = 90° - \frac{1}{2}u_0 = 390.4$ and, symmetrically, 2190.4.

The solutions in Fig. 7 show that for a particular value of $|t_0 - T_J| < 0.05$ clay the circumscribed area should degenerate into a point at $I = 180°$ and $P_{rot} = P_{crit}$. Our calculations confirmed that this was indeed so and that the minimum temporal separation of the tidal disruption from perijove yielding solutions consistent with the conditions of (34) is 0.64 hr. The range of nuclear radii that satisfy the constraints is shown in Fig. 8 as a function of the assumed effective time of disruption. The minimum nuclear radius allowed is 4.0 km, substantially larger than Scotti and Melosh's (1993) result of ~1 km.

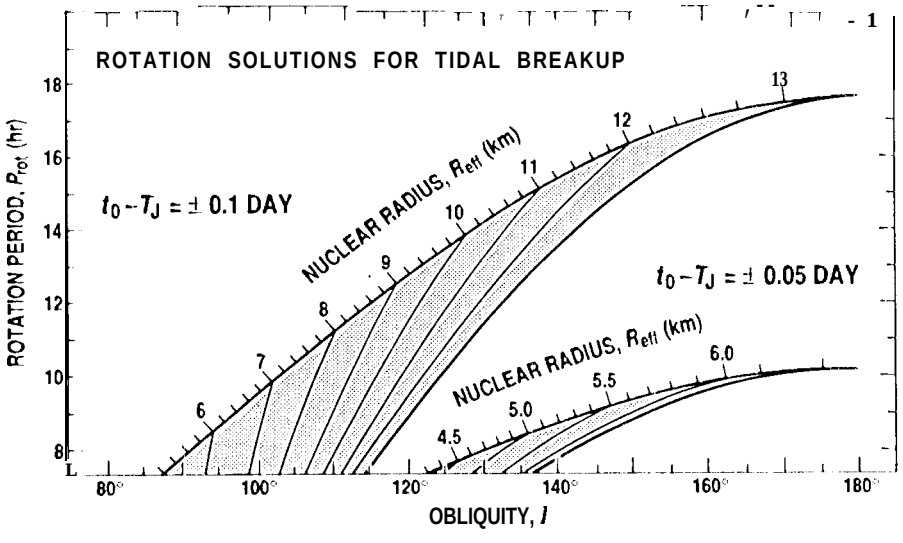

FIG. 7. Rotation solutions in a plot of the obliquity I versus the rotation period P_{rot} for $\lambda = '.25$ and for the assumed times of breakup of ± 0.05 and ± 0.10 day from perijove. The critical period P_{crit} is the ordinate for the axis of obliquities. The leaf-shaped areas for the solutions are calibrated with values of the nuclear radius R_{eff}, whose isolines are also shown.

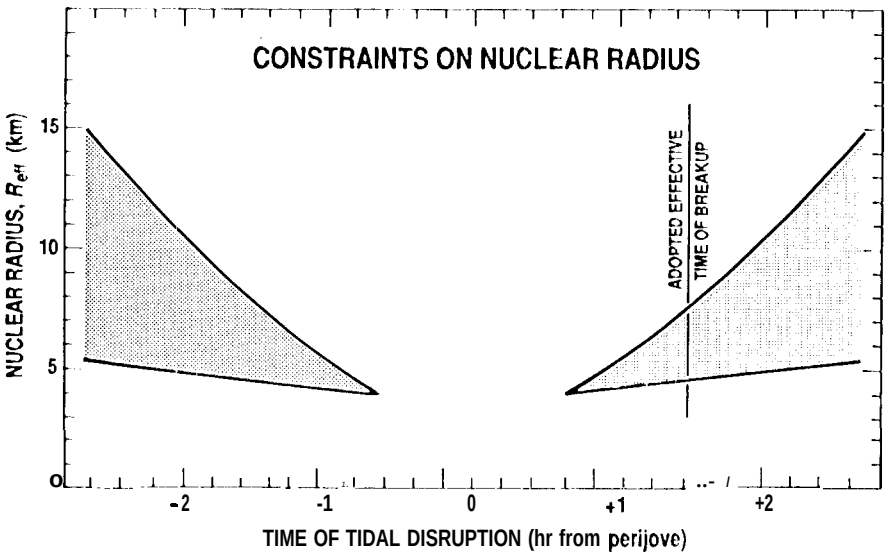

FIG. 8. Interval of nuclear radii for the parent comet that satisfy the conditions (34) versus the time of tidal disruption for $\kappa^*_{nucl} = 0.5$, $\kappa^*_{dust} = 6$, and $\lambda = 25$. The minimum implied effective radius amounts to 4.0 km. An adopted time of nuclear breakup is highlighted to show the implied limits of between 4.4 and 7.2 km on the radius of the original nucleus.

Effects of the enhancement factors κ^*_{nucl} and κ^*_{dust} are illustrated in Table 5, which lists the minimum effective nuclear radius of the parent comet, R_{eff}, calculated for an assumed time of disruption of 0.05 day from perijove. The radius was found in this case to be at least ~3 km, essentially independent of κ^*_{nucl}, but increasing with decreasing κ^*_{dust} and with increasing trail-to-train length ratio of λ. Similarly, an investigation of the enhancement factor effects carried out for an assumed obliquity of 180° and a rotation period of 7.38 hr but with no constraints set on the time of disruption showed that it was not possible to satisfy the conditions (34) with a nuclear radius smaller than ~3 km and that no solutions were found when the disruption was assumed to have occurred in the immediate proximity of perijove. Even though long-exposure images of the comet taken with wide-field cameras might yield $\lambda > 25$, Fig. 5 suggests that very few centimeter-sized and larger particulates could collisionally be accelerated to equilibrium velocities equivalent to $\kappa^*_{dust} \gtrsim 8$. Thus, values of $\kappa^*_{dust} >> 6$ are unlikely for the debris in the trails, implying that the minimum size of the parent nucleus was greater than 3 km. Similarly, enhancement factors $\kappa^*_{dust} << 6$ are unlikely because they imply minimum nucleus dimensions too large to be compatible with independent evidence (Sec. 7).

TABLE 5. Dependence of the minimum nuclear radius R_{eff} and obliquity I of P/Shoemaker-Levy 9 on the enhancement factors κ^*_{nucl} and κ^*_{dust} (for $|t_0 - T_J| = 0.05$ day, $P_{rot} = P_{crit} = 7.38$ hr, $\lambda = 25$).

Enhancement factor for debris, κ^*_{dust}	Enhancement factor for large fragments					
	$\kappa^*_{nucl} = 0.3$		$\kappa^*_{nucl} = 0.5$		$\kappa^*_{nucl} = 0.7$	
	Effective radius, R_{eff} (km)	Obliquity, I	Effective radius, R_{eff} (km)	Obliquity, I	Effective radius, R_{eff} (km)	Obliquity, I
4	7.1°	180° [a]	6.6	138°	6.5	122°
6	4.4	157	4.3	123	4.2	112
8	3.2	125	3.2	110	3.1	104

[a] No solution for $|t_0 - T_J| = 0.05$ day; listed R_{eff} and I are for the minimum $|t_0 - T_J| = 0.0577$ day.

in summary, therefore, we envision that the events experienced by 1'/Shocmaker- Levy 9 in the proximity of Jupiter on 8 July 1992 began with fissures and cracks, caused by tidal stresses propagating throughout its nucleus, whose effective radius was probably near 5 km. Perhaps even before reaching perijove, the inflicted structural failures resulted in the comet's starting to break up into a very large number of fragments of different dimensions, from microscopic particles to kilometer-sized objects. Since the debris from various locations of the original nucleus was released with different rotational velocities (on the order of 1 m/s), collisions among individual particulates became inevitable. continuing tidal fracture and collisions contributed to further fragmentation, the bulk of which apparently was not completed until after perijove. Monte Carlo simulations indicate that the collisional velocity distribution rapidly "thermalized" and developed a long tail, with typically a fcw percent of the less massive particulates reaching velocities of *more* than 5-6 times the initial rotational velocity. Simultaneously with increasing velocities and the gradual expansion of the cloud of debris, the gravitational potential of the assemblage was decreasing with time. The initial rotational velocities, not exceeding the surface escape velocity from the progenitor nucleus win-c collisionally enhanced to surpass, significantly in many case%, the surface escape velocities from even the largest fragments. However, because of the chaotic nature of the interaction among particulates, the process of collisional redistribution of individual fragments in the cloud of debris had continued until intense collisions subsided. As a result, the effective time of disruption in our model dots not coincide with the initiation of tidal fracture but, instead, essentially represents the completion of the collisions] redistribution of the debris. For the massive fragments in the train the model predicts a dynamical evolution that is different from that of the finer debris in the trails in that their equilibrium velocity distribution dots not broaden significantly and their typical post-collisional velocities arc calculated to be generally lower than their initial rotational velocities. The net result of these systematic differences is that the dust trails extend to far greater distances from the original nucleus than dots the nuclear train.

Once collisions] interaction in the cloud of particulates subsided, differential effects due to the jovian gravitational attraction and the velocity distribution among fragments could take full control of the subsequent dynamical evolution of the debris, represented schematically in Fig. 9. The jovian perturbation effects arc such that fragments that at the time of breakup were nearer the planet remain so throughout the orbit until collision. On the other hand, the effects on the orbital-velocity vector arc such that fragments with greater velocity increments in the direction of the cornet's motion have larger orbital dimensions and will collide with Jupiter later in 1994. Another noteworthy property of the nuclear train is that it always points approximately at the planet. As a result, the train was virtually perpendicular to the orbit at apojove, in mid-July 1993, but will realign itself with the orbit again as it approaches and eventually strikes the planet. The configurations of pebble- and boulder-sized debris in the trails can be described in similar terms.

The effective time of disruption), besides being the event's fundamental parameter in its own right, is also seen in Fig. 8 to provide rather severe constraints on the nuclear size of the parent comet. In Sec. 3 we remarked on the dcpcndcncc of the nuclear train's orientation on the assumed time of disruption but wc did not pursue this point any further because of the effect's relatively low temporal sensitivity. Nevertheless, wc noticed that the train's position angles calculated by Scotti and Melosh (1993) on the assumption of the disruption having taken place *exactly* at perijove did not, in their 'l'able 1, represent

the seven observations entirely satisfactorily, leaving a systematic residual of -10.0, on the average. However, because of the large scatter in the position angle residuals, from - 1°.8 to +-0°.3, we questioned the wisdom of concluding, on this evidence alone, that the disruption did not occur at perijove.

More recently, we had an opportunity to determine the nuclear train's orientation from accurate measurements of the relative positions of the 21 fragments on high-resolution images of the comet (Jewitt 1993, Weaver *et al.* 1993) taken on five elates between March 27 and July 17, 1993. The position angles are accurate to about ±0°.1 and a significant fraction of the formal error is apparently due to slight deviations of the individual fragments from a straight line, as discussed in detail later in this section. Different sets of fragments on the same image yield position angles that deviate from each other by a few hundredths of a degree, so appropriate corrections were applied to the train's position angles on the two of the five dates on which the number of measured fragments was less than 2], before models were compared with the orientation data.

A solution based on the assumption of the breakup having occurred exactly at perijove left position-angle residuals of, respectively, - 0°.26, --0°.45, -...0°,40, -.0033, and –O°.O1 on the five dates and these were considered to satisfy the observations rather poorly. Indeed, this distribution of residuals is clearly inferior to that obtained by assuming that the dynamical separation occurred a small fraction of a day after perijove. For example, the residuals are +0°.01, --0°.20, -0°.20, --0°.15, and +0°.15 for $t_0 - T_J = -0.04$ day; and + O°.1O, –O°.]1, --O°.]3, —00 09, and +0°.21 for $t_0 - T_J = +0.06$ day. In our search for the most probable effective time of disruption we required that the sum of the residuals be zero and the sum of their squares reach a minimum. Both a cubic power law representing the sum of residuals between perijove and O.] 2 day after perijove and another cubic power law representing the sum of squares of residuals between 0.02 and 0.10 day after perijove

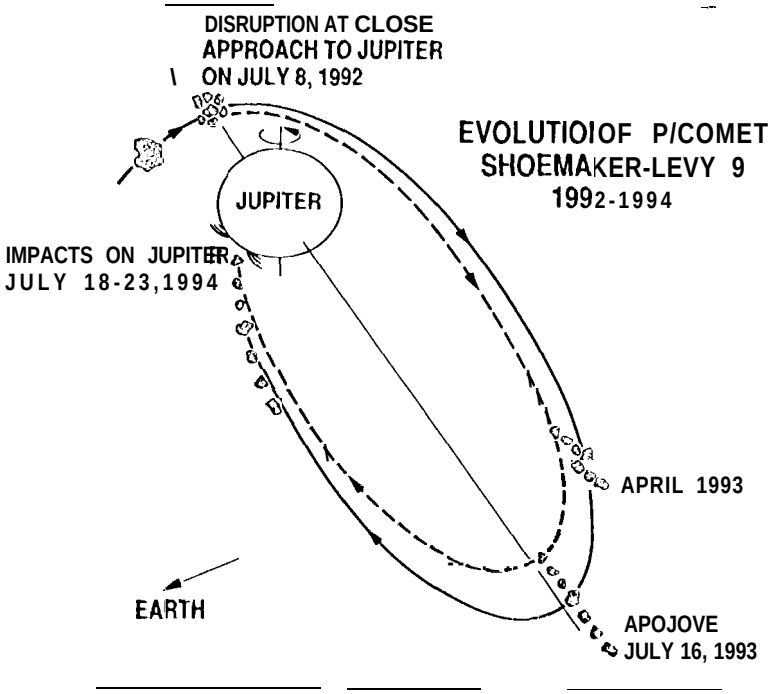

FIG. 9. Schematic representation of the tidal breakup of the parent nucleus of P/Shoemaker-Levy 9 in July 1992, the orbital evolution of its fragments, and their collision with Jupiter in July 1994. It should be remembered that the orbital dimensions are not drawn to scale and that the ratio of the apojove distance in July 1993 to the perijove distance in July 1992 is in reality equal to ~440. The sizes of Jupiter and the fragment chain are not drawn to scale either.

showed that the breakup, taken as a dynamical separation of the debris, took place most probably 0.0(308 day, or shout 1.5 hr, after perijove (Fig. 10). The uncertainty is estimated at Icss than ±0.02 day or ±0.5 hr. This time is consistent with the constraints in Fig. 8, which imply a range from 4.4 to 7.5 km for the effective radius of the original nucleus, the lower limit coinciding with the result of Sec. 7. A nominal, self-consistent model that we adopted for the nucleus and the circumstances at breakup is presented in Table 6.

From the standpoint of our analysis, the two limits on the nuclear size of the progenitor comet are equivalent. Our selection of a radius in the nominal model was strongly influenced by the results of Sec. 7, based on Weaver *et al.*'s (1 993) photometric measurements of the large fragments. This choice of the radius dictates that the spin rate of the original nucleus be very near the critics] value, so that the rapid rotation apparently assisted the tidal forces in disrupting the parent comet. The range of nuclear sizes indicated by the constraints in Fig. 8, while model dependent, is not a function of the unknown reflectivity and phase law for the fragments. For example, a plausible geometric albedo of 0.02 would result in an estimate of 6.2 km for the progenitor's nuclear radius, approximately halfway between the two limits indicated in Fig. 8. The 3σ upper limit of 2 x 10^{27} molecules/s on the comet's water production] rate (Weaver *et al.* 1993) likewise fails to provide tighter constraints on the nuclear size. Wyckoff *et al.* (]985) estimated that a water production rate equal to this limit was not reached by P/Halley until it approached the Sun to 4.7 AU. Consistent with this estimate is P/Halley's preperihelion water-production) curve by Feldman *et al.* (1 987), which predicts an H_2O rate of $\sim$6 x 10^{26} molecules/s at P/Shoemaker-Levy 9's heliocentric distance of 5.45 AU. Keller *et al.*'s (1987) estimate for the surface area of P/Halley's nucleus yields 5.6 km for its effective radius. A corresponding upper limit on the effective radius of P/Shoemaker-Levy 9 is then $\sim$1 O km, if the two comets had the

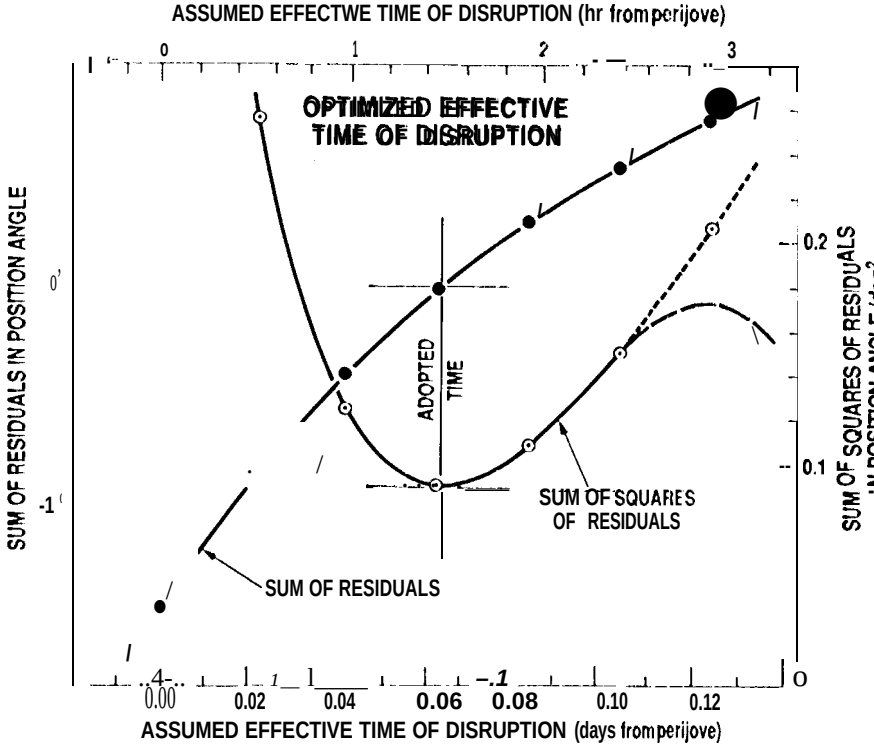

110.10. Optimization of the effective time of disruption of the progenitor nucleus of P/Shoemaker-Levy 9 based on nuclear-traill orientations determined from Jewitt *et al.*'s accurate measurements of the relative positions of 21 fragments observed by them between March 27 and July17, 1993. The curves are polynomial approxirnations of, respectively, the sum of position angle residuals and the suln of their squares.

same fraction of their nuclear surface active. However, this estimate would apply only if the comet did not split, The mass distribution) law for the large fragments that was considered in Sec. 7 implies in a spherical approximation that the sum of their surface areas should be greater than the surface area of the original nucleus by a factor of $\frac{3}{2}h_0^{1/3}$ [where h_0 is the dimensionless constant from (40)], or $\sim$2.9 times. A revised estimate for the upper limit to the nuclear radius of the parent comet is then 6 km. If less than 10% of the total surface of the fragments was outgassing at the time of the HST observation, the limit would be still higher.

'1'here is a good chance, however, that the water production of P/Shoemaker-Levy 9 is overestimated by Weaver *et al.*'s (1 993) 3σ upper limit by many orders of magnitude and that the comet's activity, if any, has for a]] practical purposes been negligible ever since discovery in March 1993. Strong evidence for this argument is offered by the results of wide-field imaging. If the comet continued to emit dust in detectable amounts, a significant fraction of the ejecta would be in the form of submicron- and micron-sized particles, since

TABLE 6. Nominal model for the nucleus and tidal fracture of P/Shoemaker-Levy 9 (P_{crit} = 7.3S hr, κ^*_{nucl} = 0.5, κ^*_{dust} = 6)

PARAMETERS OF ORIGINAL NUCLEUS (J 2000 REFERENCE FRAME)	
Effective radius, R_{eff} (km)	4.5
Rotation period, P_{rot} (hr)	7.45
Obliquity of orbital plane to equatorial plane, 1	113°
Argument of subjovian meridian at perijove, Φ	49°
Right ascension of the northern rotation pole	187°
Declination of the northern rotation pole	+36°
CIRCUMSTANCES AT TIDAL DISRUPTION	
Effective time, $t_0 - T_J$ (hr from perijove)	-11.46
True anomaly, u_0, in jovicentric orbit at the time	4820.6
Jovicentric distance at the time (Jupiter's equatorial radii)	2.79
Coefficient A (m/s)[a]	0.249
Coefficient B (m/s per km)[a]	0.069
HALF-LENGTH AND ORIENTATION OF NUCLEAR TRAIN[b]	
Radial separation parameter, $(\Delta r)_{nucl}$ (km)	+4.5
Orbital-velocity increment, $(\Delta V_{orb})_{nucl}$ (m/s)	–0.15
LENGTH AND ORIENTATION OF WEST-SOUTHWESTERN DUST TRAIL	
Adopted length factor λ	25
Radial separation parameter, $(\Delta r)_{dust}$ (kin)	–1.0
Orbital-velocity increment, $(\Delta V_{orb})_{dust}$ (m/s)	+6.41
Radiation pressure acceleration β_{end} at end point	0
LENGTH AND ORIENTATION OF EAST-NORTHEASTERN DUST TRAIL[c]	
Adopted length factor λ	17.6
Radial separation parameter, $(\Delta r)_{dust}$ (km)	+0.7
orbital-velocity increment, $(\Delta V_{orb})_{dust}$ (m/s)	–4.46
Radiation pressure acceleration β_{end} at end point	0.018

[a] For definition, see Eqs. (4).
[b] Applies to the west-southwestern] end of the train; signs of the two parameters are reversed for the east-northeastern end.
[c] One of a multitude of solutions; obtained by maximizing expression $[a(\Delta r)_{dust} + b(\Delta V_{orb})_{dust}]$.

they are the easiest to release ant] to detect optically. Representing fresh emissions subjected to solar radiation pressure, they would travel predominantly along the radius vector, away from the Sun. As projected onto the plane of the sky, the antisolar direction rotated rapidly in late March 1993 when the comet was near opposition with the Sun, the position angle having 'been (at Oh TDB) 312° on March 25, 321° on March 26, 343° on the 27th, 33° on the 28th, and 73°, 89°, and 96° on the last three days of March. By contrast, during the period from mid-April to mid-July, the position angle was almost constant, between 110° and 11 **4".** Accordingly, one should expect to see two phenomena on wide-field images of the comet, if it were active: (i) a rapid counterclockwise rotation of a bright streamer or a plume in the sector of material to the north of the nuclear train in late March and (ii) a persistent dust feature to the cast-southeast, in April-July. There is not the slightest evidence for either. It seems to us that this second point is especially lethal to the proposition] of continuing detectable activity.

The absence of such activity is supported by Weaver *et al.*'s (] 993) conclusion that the dust clouds surrounding the individual fragments in the train have apparently not been generated by a steady-state production and could be made Up of relatively large comoving particles. Furthermore, Weaver *et al.*'s comment On several of the fragments being multiple systems opens up a major issue of potentially far-reaching ramifications- the possibility of secondary, more or less spontaneous, fragmentation involving the nuclei (and quite possibly also their debris) long after the tidal disruption of the original nucleus. In Sec. 7 wc addressed specifically the problem of the two main components of the brightest fragment and showed that their separation may have taken place as late as six months after the primary breakup. Since fragmentation always entails an increase in the total cross-sectional area, the events of this kind also show up as a brightening of the fragment's envelope. The reasons for secondary fragmentation are not known, but the candidate mechanisms include possible rotational torques exerted on objects with major structural cracks that did not split during the primary bi eakup. Except for the absence of ejecta expanding at rates comparable with the sublimation velocity, the resulting effects mimic erratic activity and are entirely consistent with the observed temporal variations in the brightness of the individual fragments.

Before employing the nominal model to predict the comet's future behavior, we summarize the results of its comparison with observations available at this time. The 21 individual fragments reported by Jewitt (1 993) are identified in order of their position along the train, the easternmost fragment (Jewitt's #/21) being assigned the letter A and the westernmost fragment (Jewitt's #/I), the letter W (with] and O not used). The brigl ntest fragment, identical with Jewitt's ##7, is identified as Q. The model represents the five high-precision orientation data on the nuclear train (Jewitt, Weaver) with a mean error of ±0°.13 in position angle and four high-precision data on the train's length (Jewitt) with a mean error of ±0.1 O arcsec. Since Weaver *et al.* did not measure the two easternmost fragments, A and B, the train's length could not be determined. However, if scaled from the measured fragments C and W, a somewhat disturbing difference of about – 0.2 arcsec is suggested in the sense Weaver minus Jewitt.

An interesting finding is that the formal error of the train's orientation calculated from the 11 fragments measured by Weaver *et al.* is not smaller than that calculated from the same selection of fragments measured by Jewitt. It appears that the results do not depend on the image definition, which is superior on the HST frames, and that therefore the

forma] error in the train's orientation reflects true deviations of *the individual fragments from perfect* alignment. These deviations are not systematic in the sense that the string of fragments would deviate from the great circle, since the polynomial representations always showed the quadratic term to be meaningless. Instead, some fragments were found to have a tendency toward being systematically to the north of the mean line, others to the south of it. Of the 11 fragments measured on all five dates, E and 1, were always to the south of the mean line by, respectively, 0.05 and 0,11 arcsec, on the average. Considering only Jewitt's measurements of the 21 fragments, six pieces—B, F, J, M, 1', and T (the last not measured in July 1993)---were always to the north of the mean line and nine- -- A, D, E, G, H, K, L, R, and W--always to the south. Seven of these 15- A, B, D, J, M, P, and T- arc not among Weaver *et al.*'s 11 brightest ones and three of them deviated from the mean line very significantly: B by 0.36 arcsec, T by 0.25 arcsec, and M by 0.24 arcsec. In the light of our findings, these results arc interpreted as apparent evidence of a scatter in the effective times of disruption for the individual pieces.

A property common to all the fragments that is mentioned by Weaver *et al.* also appears to be qualitatively consistent with our model. It is a dust coma that surrounds each of the objects, accounting for most of the light and displaying radial profiles much flatter than those characteristic of steady-state dust production and constant outflow velocities. In Fig. 5 we show that a small but non-negligible fraction of the debris, including sizable chunks, is collisionally decelerated to extremely low velocities and could easily get trapped into gravitationally bound orbits about one of the large fragments. The collisional model thus provides a mechanism for Weaver *et al.*'s hypothesis of co-moving debris. Depending upon each fragment's mass, these orbits could become qllasi-stable except in the immediate proximity of Jupiter (Sec. 4), the spatial density of t}$_{\text{lc}}$ trapped debris varying much less steeply than the inverse square of distance from the fragment's center out to the boundary of its sphere of influence.

Comparison of the parameters $(\Delta r)_{\text{nucl}}$ and $(\Delta V_{\text{orb}})_{\text{nucl}}$ in '1'able 6 with $\Delta r|_{\Delta V_{\text{orb}}=0}$ and $\Delta V_{\text{orb}}|_{\Delta r=0}$ from Eqs. (1) shows that the extent of the nuclear train is due primarily to the radial-separation effect. The effect in the orbital velocity accounts in this model for less than 40% of the former and works in the opposite direction. By contrast, our interpretation of the dust-trail lengths implies a dominant velocity effect. The observations of the west-southwestern dust trail in Table 2 suggest an average position angle of 257° ± 2°; the model predicts 2570.3 on the first listed date, March 26, and 2560.4011 the last, May 25, 1993. The reported maximum length, ~10.5 arcmin in late March, requires a separation velocity of more than 6 m/s in the direction of the orbital motion (Table 6). The trail's alignment with the nuclear train implies the absence of a measurable effect of solar radiation pressure on the particulates, whose dimensions arc estimated to range from several centimeters to several hundred meters. And since the collisionally acquired separation velocity distribution) is shown in Fig. 5 to be strongly mass dependent, we conclude that the characteristic particle size decreases systematically along the trail from the mentioned upper limit, near the nuclear train to the lower limit at the trail's far end.

If the parent comet had a spherical nucleus that would disrupt in a fairly organized fashion prescribed by the theory of tidal fracture, the east-northeastern and west-southwestcrri trails should be symmetrical with respect to the nuclear train. This symmetry would be reflected in their equal lengths and extension in the same direction. In reality, the east-northeastern trail was always observed to be the significantly shorter of the two, perhaps

slightly less sharply defined, and pointing somewhat to the north of the extended direction of the west-southwestern trail and the nuclear train (Fig.]). The observations listed in Table 2 show that the bend of the shorter trail was on the average 4° ± 2° in March-May 1993, its position angle being 73° rather than 77°. Its reported length was on the average 0.63 ± 0.05 the length of the west-southwestxxm trail. These deviations from the symmetry appear to provide evidence for an irregularly shaped nucleus of the parent cornet, and possibly also for nonuniform physical conditions during the breakup and in the subsequent collisional environment, Since the chaotic nature of the collisional process rules out any one-to-one correlation between a minor fragment's initial location in the original nucleus and its location in the dust trail at a given time, it is not possible to pinpoint the exact source of the asymmetry between the two trails. Nevertheless, the observational evidence leads to two conclusions: (i) the shorter length of the ca.st-northeastern trail indicates that the regions of the original nucleus that were the source of the debris in this feature were generally deficient in mass compared with other regions and (ii) the different orientation of the east-northeastern trail suggests that centimeter-sized and larger particulates are largely absent from it. This second conclusion is quantified in Fig. 11, which shows that at the end of March 1993, the largest particles situated 2 and 5 arcmin from the nuclear train along the east-northeastern trail were subjected to solar radiation pressure accelerations β of, respectively, 0.005 and 0.012 the solar attraction. The corresponding diameters of these particles arc 1.2 and 0.5 mm, if their density is 0.2 g/cm^3, or 0.24 and 0.1 mm, if 1 g/cm3 The trail's deviation from the syndyname $\beta = 0$ also affects the length factor λ, as is apparent from Fig. I 1. Instead of $\lambda \simeq 15$, the more appropriate value is now $\lambda = 17.G$, as listed in 'J'able 6.

The relatively flat mass distribution, $h(m)\,dm \propto m^{-1}\,dm$, the evidence for whit.1] among the largest fragments was presented in Sec. 7 and whose validity for fragments as small as ~)cbblc-sized plays a critics,] role in our collisional model (Sec. 5), is inconsistent with the huge cross-sectional area of the dust inferred in Sec. 4 from the comet's reported integrated brightness (Fig. 4). It is apparent from Fig. 1 that the debris in the dust trails contributes much less light than the material distributed in the vast volume of space projecting in the northerly direction from the trails. As illustrated in Fig. 11, our model shows that this whole space is a *tail* region, populated by particulates whose motions arc appreciably affected by solar radiation pressure, and that the angular distance from the train/trails is a measure of the particle acceleration β exerted by this radiation pressure, The apparent discrepancies in observational evidence are reconciled, if the mass distribution of the debris is assumed to become significantly steeper than $m^{-1}\,dm$ for particles smaller than several centimeters in radius. A numerical exercise shows tentatively that a mass distribution somewhat st eeper than $m^{-2}\,dm$ could explain the inferred large cross-sectional area of fine dust, without affecting the conceptual validity of the collisions] mode] and the estimate for the size of the original nucleus presented in Sec. 7. Fine dust, released at, or shortly after, breakup from (or along with) the fragments populating the train/trails, is predicted to line up, on the comet's images taken at the end of March 1993, along a position angle of ~280°, which matches closely the reported orientation of the tails issuing from the major fragments ('l'able 2). As shown in Fig. 11, each such line is described by the "parent" fragment's angular distance, Λ^*, reckoned along the nuclear train (and/or its extension) from its middle, or, equivalently, by a scaled distance $\lambda^* = 2\Lambda^* / \Lambda_{nucl}$, defined in the same fashion as the length parameter λ.

The brightest portion of the tail region, confined in Fig. 1 to a relatively narrow band along the northern side of the nuclear train, is made up of particles the smallest of which are not more than ~150 μm in size and subjected to radiation pressure accelerations of ~2% of the solar attraction. By contrast, particles populating the areas most distant from the trails, in the northwestern corner of Fig. 1, are about 15 μm or less in size and subjected to radiation pressure accelerations of $\gtrsim$20% of the solar attraction. Apparently, the comet's debris extends well beyond the limits of the fields in Figs. 1 and 11, both in the direction of increasing radiation pressure (that is, decreasing particle size) and "(sideways", toward scale distances $\lambda^* > \lambda$, since equilibrium velocities acquired collisionally by microscopic grains should, on the average, be higher than those of pebble-sizecl and larger particulate.

We close this section with four comments. Even though the existing sets of orbital elements for P/Shoemaker-Levy 9 arc not accurate enough to study the long-term evolution of the cornet, we made an attempt to integrate its motion back in time and found that while

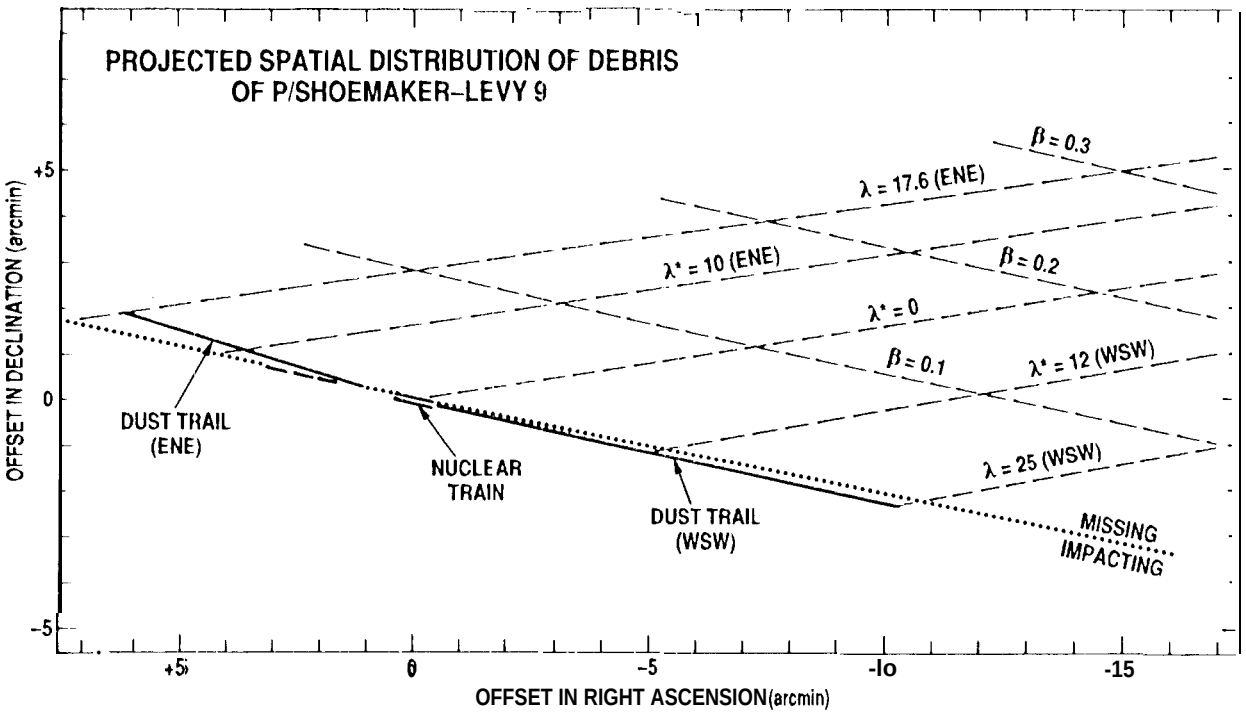

FIG. 11. Schematic chart of the modeled spatial distribution of the debris of P/Shoemaker-Levy 9 on 1993 March 30.31 UT, projected onto the plane of the sky. The offsets in right ascension and declination are reckoned in arcminutes from the middle of the nuclear train that is represented by the short double bar. The west-southwestcrll and the east-northeastern extensions of the train arc the two trails, shown by heavy lines. Their "reference" lengths are, respectively, 10.5 and 6.3 arcmin, corresponding to $\lambda = 25$ and 17.6, at position angles of 257° and 73°. The latter trail's orientation calculated on the assumption of no radiation pressure effect is shown by the heavy da.shed line. The light dashed lines running parallel to the dust trails are syndynames, or isolines of a constant particle acceleration β due to solar radiation pressure, expressed in units of the solar gravitation] acceleration. The light dashed lines pointing toward the west-northwest, at a position angle of ~280°, are the predicted loci of fine particles released, at the time of breakup, from (or along with) the objects located at the intersection of these lines with the train/trail and are identified by their scaled distance A*. The slope of these lines matches closely the observed tail orientation of the major fragments (Fig. 1 and 'l'able 2). Finally, the dotted line, slightly inclined to the train and the trails, indicates the boundary separating the population of fragments, to the south, that will collide with Jupiter, from the debris that will miss the planet in 1994.

the comet was in orbit about Jupiter for at least several revolutions, there was no close approach prior to that in 1992. The previous minimum perijove distance was ~130 Jupiter's radii in 1989, implying that before] 992 the comet experienced maximum tidal stresses 1 0^{-5} to 10^{-6} times smaller than those on 8 July 1992 and that it therefore could not have split tidally before then.

We call attention to a potentially significant role of shape on the effective radii of both the original nucleus and its fragments calculated from cross-sectional areas. The assumption of spherical shape is convenient but demonstrably incorrect. Considering the tendency for tidal fracture to proceed along planes that arc normal to the comet-- planet line (Sec. **3),** a disk-like shape should be more appropriate for the fragments, even if the original nucleus were spherical. A disk-shaped fragment of a radius $R_{\rm disk}$ and height $H_{\rm disk}$ has an average cross- sectional area of $\frac{1}{2}\pi R_{\rm disk}^2(] + h_{\rm disk})$, Where $h_{\rm disk} = H_{\rm disk}/R_{\rm disk} \ll 1$ to account for the large number of major fragments. Setting this expression equal to the cross-sectional area, of a sphere, $\pi R_{\rm eff}^2$, yields $R_{\rm eff} = R_{\rm disk}\sqrt{\frac{1}{2}(1 + h_{\rm disk})}$ and with a conservative estimate, $h_{\rm disk} \simeq 0.3$ to 0.4, we have $R_{\rm eff} \simeq 0.8R_{\rm disk}$, so that the spherical approximation underestimates the size. The effect is even more pronounced in volume considerations, from whi ch one finds $R_{\rm eff} = R_{\rm disk}\sqrt[3]{\frac{3}{4}h_{\rm disk}}$ and, with the above estimate fOr $h_{\rm disk}$, $R_{\rm eff} < 0.7R_{\rm disk}$.

Melosh and Schenk (1993) suggested that crater chains on Ganymede and Callisto are impact signatures of comets that had tidally split near Jupiter prior to their collisions with one of the two satellites. We regard this hypothesis as credible because fo, the massive fragments of l'/Shoemaker- Levy 9 the jovian radial differential Perturbations, which play a major role in the Melosh- Schenk scenario, appear to dominate the effects of the collisional particle velocity distribution. Our point of disagreement with Scotti and Melosh's (1 *993)* model is therefore not primarily the issue of relative magnitudes of the radial-separation and velocity-field effects on the formation of the nuclear train, but rather the authors' invalid assumption that the breakup (meaning the initiation of a systematic separation of the fragments) occurred *exactly* at perijove. We confirmed Melosh and Schenk's (1 993) conclusion) that rotational bursting *alone* could not explain the high degree of linearity of the! observed crater chains. However, with the radial-separation effect dominating and with initial rotational velocities of kilometer-sized fragments collisions.lly randomized ant] their magnitudes diminished ($\kappa^*_{\rm nucl} << 1$), wc doubt that the involved rotatiol)-velocity effect would show up prominently enough in the crater chains.

Finally, the low velocities (a few m/s) of the debris arc comparable with velocities that theories of solar-system formation often accept as low enough to support accretion of material and growth of sizable objects in the primordial solar nebula (cf. Bailey *et al.* 1990 for a review). Hartmann's (1 978) quoted laboratory experiments were undertaken with these issues in mind. Considering especially the high spatial density in the cornet's post- breakup environ ment, one wonders how realistic arc these hypotheses of the solar system origin when based on such accretion concepts. Accretion does not appear to work efficiently in the presence of nearby massive perturbers and these concepts must therefore explain how slowly accreting cometesimals avoided encounters with such objects during the entire period of their gravitational collapse. While we cannot exclude the possibility that some limited reassembling of the debris may have occurred locally in the dust cloud of P/Shoemaker- Levy 9 after its breakup, the observations show beyond doubt that the ultimate result of low-velocity particle interactions is a thoroughly disintegrated object.

9. PREDICTIONS FOR 1994

Our predictions for 1994 arc based on the nominal model presented in '1'able 6 and fall into two categories: (i) ephemerides of the future motions of the debris and (ii) information on the impacts.

Ephemerides. I'able 7 offers the predicted apparent length and orientation of the nuclear train between December 19, 1993 and July 17, 1994. The train's length is defined as the angular distance between the fragments A and W, observed by Jewitt *et al.* between March 27 and July 17, 1993. The orientation of the train is defined as the position angle of the great circle fitted through the 21 fragments. Although the orbital elements arc based on astrometric observations of the train's midpoint, the calculations show that this reference point determined from the 1993 observations will '(travel" along the train and that its distances from the fragments A and W will not remain equal in 1994.

'J'able 8 lists the predicted separations of the fragments A through P ancl R through W from the brightest fragment Q along the nuclear train for the same period of time as Table 7. 'l'his ephemeris should prove useful both for fragment identification when the comet reappears after its conjunction with the Sun and for fut urc improved pred ict ions, especially in the light, of Weaver *et al.*'s (1 *993)* remark on the multiplicity of several of the fragments and the possibility of secondary fragmentation events (Sees. 7 and 8). Note that, by definition, the sum of projected separations of the fragments A and W from Q in ~'able 8 is equal to the train's length in '.l'able 7.

Table 9 presents the predicted orientations and characteristic lengths of the two trails and the tails. The trail endpoints arc defined by the adopted lengths of 6.3 and 10.5 arcmin on March 30, 1993 for the east-northeastern and the west-southwestern trails, respectively. The ephemeris for the east-northeastern trail is calculated with $\beta_{end} = 0.018$ (Table 6). Since the effect of solar radiation pressure was determined from a subtle 4° deviation in position angle and is therefore uncertain, scaled predictions for this trail arc also given for the case of $\beta_{end} = O$ to illustrate the effect's changing signature in the coming months. Still, the prediction in '1'able 9 dots not describe the east-northeastern trail's expected behavior in sufficient detail. The calculations show that near the nuclear train this trail always starts off in the first quadrant, but during June and July 1994 it will develop a sharp, V-shaped turn at its tip, swinging in the opposite direction to join the other trail and the tails to

TABLE 7. Predicted apparent length and position angle for the nuclear train of P/Shoemaker-Levy 9 (reference frame J2000).

Date[a] 0h TDB 1993/94	Length (arcsec)	Position angle	Date[a] 0h TDB 1994	Length (arcsec)	Position angle	Date[a] 0h TDB 1994	Length (arcsec)	Position angle	Date[a] 0h TDB 1994	Length (arcsec)	Position angle
Dec 19	121	245°.9	Apt 8	268	242°.1	June 7	414	244°.1	July 7	617	242°.8
Jan 8	136	244.1	18	288	242.6	12	433	244.0	9	651	242.5
28	156	242.6	28	310	243.0	17	455	243.9	11	694	242.2
Feb 17	181	241.6	May 8	333	243.5	22	480	243.8	13	751	241.9
Mar 9	211	241.3	18	357	243.8	27	513	243.5	15	834	241.3
29	247	241.7	28	383	244.0	July 2	555	243.2	17	976	240.5

[a] TDB is barycentric dynamical time; in October 1993, TDB ≃ UT + 60^s.2.

TABLE 8. Predicted projected separations among the 21 fragments of P/Shoemaker–Levy 9.

Date 0^h TDB 1993/94	Fragment's separation (arcsec) from brightest fragment Q																			
	Toward east-northeast														Toward west-southwest					
	A	B	C	D	E	F	G	H	J	K	L	M	N	P	R	S	T	U	V	W
Dec 19	88	82	78	73	70	62	55	44	38	31	20	13	9	5	9	18	20	24	30	33
Jan 8	99	92	88	83	79	70	62	50	43	35	22	14	10	5	10	20	23	27	34	37
28	114	106	100	95	91	80	71	57	49	40	26	16	12	6	11	23	26	31	38	42
Feb 17	132	123	116	110	105	93	83	66	57	46	30	19	14	7	13	27	30	36	45	49
Mar 9	154	144	136	129	123	109	97	78	66	54	35	22	16	8	15	31	35	42	52	57
29	180	168	159	151	144	127	113	91	78	63	41	26	19	9	18	36	41	49	61	67
Apr 8	195	182	172	163	156	137	122	98	84	68	44	28	20	10	19	39	44	53	66	73
18	210	196	186	176	168	148	132	106	90	73	47	30	22	11	21	42	47	57	71	78
28	226	211	200	189	181	159	142	114	97	79	51	32	23	12	22	46	51	61	76	84
May 8	243	227	214	203	194	171	152	122	104	84	54	34	25	12	24	49	55	65	82	90
18	261	243	230	218	208	184	163	131	112	90	58	37	27	13	25	52	59	70	87	96
28	280	261	247	234	224	197	175	141	120	97	63	40	29	14	27	56	63	75	94	103
June 7	303	283	268	253	242	213	190	152	130	105	68	43	31	15	29	60	68	81	101	111
12	317	296	280	264	253	223	198	159	135	110	71	45	32	16	31	63	71	85	105	116
17	333	310	294	278	265	234	208	166	142	115	74	47	34	17	32	66	74	89	110	122
22	352	328	311	294	281	247	220	176	150	121	78	49	36	18	34	70	78	93	116	128
27	377	351	332	314	300	264	234	188	160	129	83	52	38	19	36	74	83	99	123	136
July 2	409	381	360	340	325	286	254	203	173	140	90	57	41	20	39	80	89	107	133	146
7	457	425	402	379	362	318	282	225	191	154	99	62	45	22	43	88	98	117	146	160
9	483	449	424	400	382	335	297	237	201	162	104	66	48	24	45	92	103	123	152	168
11	517	470	453	427	407	357	316	251	214	172	110	69	51	25	47	97	108	129	161	177
13	563	522	492	463	442	386	341	271	230	185	118	74	54	27	50	103	115	138	171	188
15	631	583	548	515	490	427	377	298	252	202	129	81	59	29	55	112	125	149	185	203
17	752	689	644	603	571	494	433	339	286	229	145	91	66	32	61	124	138	165	204	224

form a gradually folding sector of material toward the west-southwest. The ephemeris for the tail region refers to a syndyname of $\beta = 0.02$, which approximately defined the outer boundary of the feature's brightest portion in late March 1993. Because of the continuing dispersion of the debris in space, the trails and the tail region may appear, in 1994, to be fainter and/or shorter than predicted or they may not be detected at all.

Impacts. The orbital elements for the midpoint of the nuclear train (~'able 1) yield a nominal collision time with Jupiter of 1994 July 21.20590 TDB (light time not included), whose uncertainty has a standard deviation, σ, of ± 7.1 hr. As time proceeds and more astrometric observations arc added to the orbit solution, the impact time prediction will become more accurate. To predict the rate of decrease in the impact time uncertainty, we simulated future astrometric observations. We assumed one astrometric observation every three days starting December 29, 1993, and daily observations in the last three days before impact. The assumed observation accuracy was ± 1.3 arcsec (1σ). 'J'able 10 presents the impact time uncertainty as a function of the date of the last astrometric observation; the first line of the table indicates the current uncertainty.

TABLE 9. Predicted apparent length and orientation for the dust trails and the tail region of P/Shoemaker-Levy 9.

Date 0^h TDB 1993/94	East-northeastern trail, $\beta_{end} = 0.018$		East-northeastern trail, $\beta_{end} = 0$ (assumed)		West-southwestern trail ($\beta_{end} = 0$)		'l'ail region (syndyname $\beta = 0.02$)	
	Length (arcmin)	Position angle	Length (arcmin)	Position angle	Length (arcmin)	Position angle	Length (arcmin)	Position angle
Dec 19	12	45°	16	66°	24	246°	9	276'
Jan 8	13	42	18	64	27	244	11	275
28	15	39	20	62	31	243	13	273
Feb 17	17	39	24	61	35	242	15	272
Mar 9	20	40	28	61	41	242	17	271
29	24	44	34	61	4'7	242	19	269
Apr 8	26	46	37	62	51	242	20	268
18	29	49	40	62	54	243	21	267
28	32	51	44	63	58	243	21	266
May 8	35	53	48	63	61	244	22	265
18	39	56	54	63	65	244	22	263
28	43	57	63	63	68	245	23	261
June 7	50	59	67	59	71	245	24	260
12	54	60	49	56	73	245	24	259
17	61	61	33	51	75	245	25	258
22	71	61	20	41	77	245	26	257
27	49	58	9	6	80	245	27	255
July 2	30	54	12	289	83	244	28	254
7	13	39	23	265	86	244	30	253
9	7	13	28	261	88	244	31	252
11	6	305	33	258	90	244	32	251
13	12	271	38	256	92	244	33	251
15	19	260	44	254	94	244	35	250
17	26	254	50	253	97	243	37	249

TABLE 10. Impact time uncertainty as a function of time.

Date of last observation	Time before impact	Impact time uncertainty (1σ)
1993 July 11	~1 yr	±7.1 hr
1994 Mar 26	~4 mo	±26 min
Apr 23	~3 mo	±23 min
May 20	~2)110	±18 min
June 13	~5½ wk	±13 min
July 14	~1 wk	±7 min
)994 July 21	~6 hr	±3 min

While the. absolute uncertainty in the impact times of the 2] fragments is likely to be somewhat larger than the uncertainty for the train's midpoint, their errors relative to the midpoint's reference time arc considerably smaller, typically ±10 or so minutes. The relative impact times arc listed in Table 11. The impacts arc predicted to occur on the far side of Jupiter as viewed from Earth, at jovigraphic latitudes ranging from -410 to –47° (equivalent to jovicentric latitudes between --37° and –43°) and at meridian angles

TABLE 11. Predicted relative times of impact for the 21 fragments of P/Shoemaker-Levy 9 and probabilities of favorable satellite configurations.

Fragment	impact time[a] (days)	Probability of favorable satellite configuration[b]			
		10	Europa	Ganymede	Callisto
A	-2.7303-0.006	0.47	0.05	0.02	1.00
B	-2.4673.0.008	0.76	0.24	0.00	1.00
c:	–2.271 ± 0.006	0.79	0.47	0.00	1.00
D	-2.084 ± 0.009	0.66	0.71	0.00	1.00
E	– 1.9404 0.004	0.48	0.85	0.00	1.00
F	--1.56740.012	0.10	0.99	0.00	1.00
G	–1.260 ± 0.006	0.14	0.98	0.00	1.00
H	-0.767 ± 0.004	0.69	0.68	0.00	1.00
J	-0.4733.0.011	0.78	0.30	0.00	0.98
K	–0.150 ± 0.004	0.46	0.05	0.02	0.82
L	+0.344 4.0.004	0.05	0.00	0.32	0.23
M	+0.675± 0.016	0.29	0.02	0.74	0.03
N	+ 0.830+ 0.004	0.48	0.05	0.88	0.01
P'	+1.040 ± 0.011	0.72	0.17	0.97	0.00
Q'	+1.245 ± 0.005	0.79	0.40	0.99	0.00
R	+ 1.640+ 0.006	0.43	0.86	1.00	0.00
s	+2.057± 0.014	0.06	0.99	1.00	0.00
T	+2.155 ± 0.012	0.06	0.99	1.00	0.00
u	+ 2.336+ 0.009	0.17	0.98	1.00	0.00
v	+2.605± 0.016	0.48	0.87	1.00	0.00
W	+2.745 40.006	0.65	0.74	1.00	0.00

[a] Relative to the midpoint's reference time, for whit), ou current estimate is 1994 July 21.24 0.3(1 o) TDB.
[b] Occultation.s by Jupiter not taken into account.
[c] Brightest fragment.

ranging from 34° to 37° past local midnight. The Sun-fragment–Jupiter center angles at impact will vary between *510* and *57°* and the Earth- Jupiter center-fragment angles between 117(' and 122°. We caution that the tabulated sequence of impacts is based on the current knowledge of 2] major fragments. If some of the fragments began to develop into multiple systems, as suggested by Weaver *et al.* (1993), Tables 8 and 11 may soon require numerous revisions and/or additions,

The predicted impact-time distribution for the 2] fragments is plotted in Fig. 12, showing peaks at both ends of the nuclear train and a broad minimum in the middle. The histogram, reflecting the distribution of fragments along the train, is presumed to be a signature of tidal fracture of the comet's progenitor nucleus and will hopefully contribute to a better understanding of the breakup mechanism, even though its interpretation-- save unlikely *ad hoc* models, such as a dulnbbcll-shaped or a binary nucleus- does not appear to be straightforward, Another interesting feature of Fig. 12 is the apparent tendency for most of the fragments to clump into groups; note, in particular, the threw clusters of five fragments each, A-N, I,- Q, and S-W.

There is general interest in observing reflections, from the surface of favorably located jovian satellites, of the luminous energy released during the fireball explosions, brought about by the individual fragments plunging into the planet's atmosphere (e. g., Sekanina 1993). Since the scatter in the impact sites of the 21 events in the nonrotating jovicentric coordinate systcm is only a few degrees, the impact times account for virtually all the uncertainty involved. At present this uncertainty is still too large to predict with confidence all the satellite configurations relative to the local horizon at the critical times. This is particularly true for 10 and, to a lesser degree, Europa. To assist in the planned observing

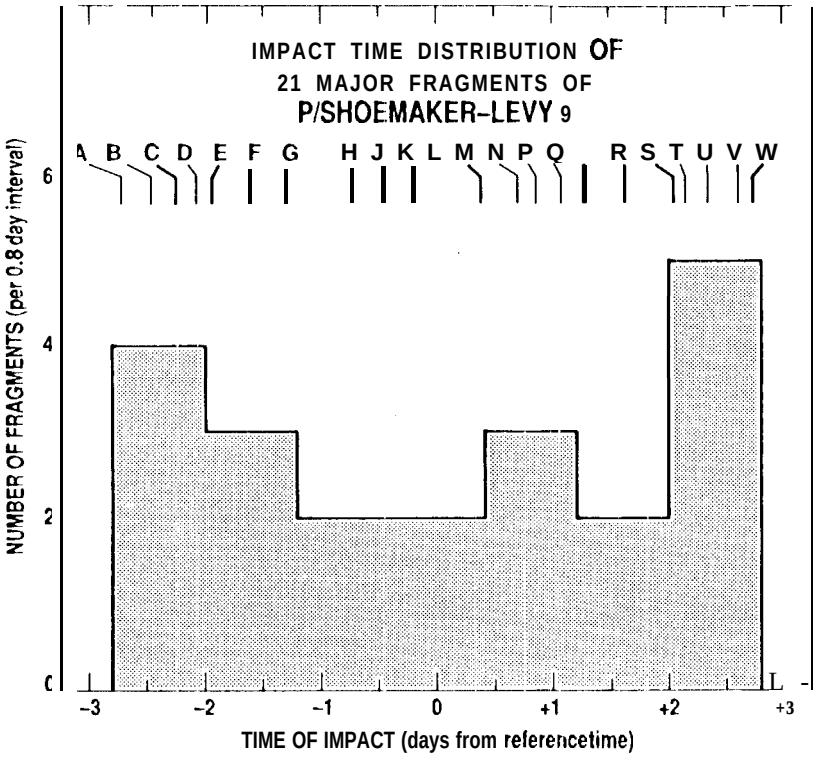

FIG. 12. Histogram of the impact times predicted for the fragments of P/Shoemaker–Levy 9. Our best estimate for the reference time, 1994 July 21.2 ± 0.3 (1σ) TDB, is subject to future refinements. The upper part of the figure depicts the impact events of the 21 fragments by their letters. The heaviest mark identifies the brightest fragment Q, whereas the medium heavy marks show tbc 10 additional fragments measured by Weaver *et al.* (1993) and the light ones the 10 remaining fragments.

efforts to the extent possible under the circumstances, we established, separately for each of the four Galilean satellites, the *probability* of favorable conditions for each of the 21 events. If Θ_{imp} and ϕ_{imp} are the nominal values for the meridian angle (reckoned cast ward from the local midnight) and the jovigraphic latitude at the site of the explosion, a satellite will be above the horizon when it is situated within an orbits] arc bounded by the meridian angles $\Theta^- = \Theta_{imp} - \Delta\Theta$ and $\Theta^+ = \Theta_{imp} + \Delta\Theta$, where

$$\cos \Delta\Theta = \frac{R_J\sqrt{1 - [1 - (1-\epsilon_J)^2]\sin^2\phi_{imp}}}{r_* \cos\phi_{imp}}, \qquad (42)$$

R_J is Jupiter's equatorial radius, ϵ_J its polar flattening, and r_* the satellite's orbits] radius. An impact time uncertainty, defined by its standard deviation σ, can conveniently be measured in terms of a standard deviation σ_Θ of the equivalent uncertainty of the meridian angle of a satellite that orbits in the planet's equatorial plane. If the satellite's calculated meridian angle at the nominal impact time is Θ_*, the likelihood that it will be above the local horizon at the actual impact time is measured by the area of the probability curve, which is centered on Θ_*, whose shape is characterized by the standard deviation σ_Θ, and whose boundaries, given by Θ^- and Θ^+, are in general asymmetrically situated with respect to Θ_*. Disregarding occultations by Jupiter, the probability Π of a favorable configuration of a satellite whose synodic orbital period about Jupiter is P_{syn} is

$$\Pi = \text{Const} \int_{\Theta^-}^{\Theta^+} \exp\left[-\frac{(\Theta - \Theta_*)^2}{2\sigma_\Theta^2}\right] d\Theta, \qquad (43)$$

where $\sigma_\Theta = (2\pi/P_{syn})\sigma$, the current value of σ is 7.] hr (Table 10), and the normaliza tion constant is determined by a condition that $\Pi = 1$ when the integration is carried out from $-\infty$ to $+\infty$. Defining $\Delta\Theta_* = \Theta_* - \Theta_{imp}$, the expression for Π can be rewritten thus:

$$\Pi = \frac{1}{2}\left[\text{erf}\left(\frac{\Delta\Theta + \Delta\Theta_*}{\sigma\sqrt{2}} \cdot \frac{P_{syn}}{2\pi}\right) + \text{erf}\left(\frac{\Delta\Theta - \Delta\Theta_*}{\sigma\sqrt{2}} \cdot \frac{P_{syn}}{2\pi}\right)\right], \qquad (44)$$

where $\Delta\Theta$ from (42) and $\Delta\Theta_*$ are in radians, P_{syn} is in the same units as σ, and the probability integral is

$$\text{erf}(\xi) = \frac{2}{\sqrt{\pi}} \int_0^\xi \exp(-y^2)\, dy. \qquad (45)$$

The effect of inherent indeterminacy of the solution for satellites whose orbital period is not at least a factor of 10 or so greater than the standard deviation σ of the uncertainty in the impact time is reflected in the maximum and minimum probabilities $\Pi_{max} < 1$ and $\Pi_{min} > 0$. I'heir values are obtained by setting $\Delta\Theta_*$ in (44) equal to O and $\pm\pi$, respectively. With the relevant constants for Jupiter and its satellites taken from Seidelmann (1 992), we find $\Pi_{max} = 0.80$ and $\Pi_{min} = 0.04$ for 10, but $0.993 < \Pi_{max} < 1$ and $\Pi_{min} < 0.001$ for the other three satellites. We also point out that an event observable at a 1σ confidence level corresponds to $\Pi = 0.84$, at a 2σ level to $\Pi = 0.977$, and at a 3σ level to $\Pi = 0.999$. No such events can at present be predicted for 10 and no 3σ level events for Europa.

The calculated probabilities 11 for the 21 events are listed in columns 3-6 of '1'able 11. The probabilities referring to events predicted at $\gtrsim 2\sigma$ confidence level are underlined. One can see from the table that Callisto is expected to be favorably situated for the early impacts, which will involve the fragments A-11 and perhaps also J, while Ganymede for the late impacts, involving the fragments R- W, perhaps also P and Q, and possibly even N. '1'here is a good chance that observations of Europa could be used to gain information on the impacts of the fragments F, G, S, T, and 11, and pa-haps even E, R, and V. Although Io will be situated favorably for at least a few impacts, their predictions arc at this time still uncertain. The possible candidates arc the fragments C, J, and Q (the brightest one). At present it appears that, in terms of the configuration of the Galilean satellites, the least favorable circumstances will pertain to the impacts of the fragments K- M, although this could change if our absolute impact times are in error by more than 10.

The impact circumstance for the debris outside the nuclear train arc more diverse than the conditions for the 2] major fragments, as seen from a summary in q'able 12. Our calculations indicate that only a small fraction of the volume occupied by the comet's material contains debris that will collide with Jupiter in 1994. These particulates arc subjected to radiation pressure accelerations not exceeding a critical value β_{crit}, which depends on the scaled distance λ^*. For the comet's image taken on March 30, 1993 (Fig. 1), the boundary between particles that will strike the planet in 1994 and those that will miss it is represented in Fig. 11 by a dotted curve, which can very closely be matched by the following relation between λ^* and the critical radiation pressure acceleration β_{crit}:

$$\beta_{crit} = 0.00345 \mp 0.01968 \left(\frac{\lambda^*}{100}\right) + 0.004136 \left(\frac{\lambda^*}{100}\right)^2, \qquad (46)$$

where the upper sign of the linear term applies to the east-northeastern trail and the lower sign to the west-southwestern trail. however, along the east-northeastern trail this formula is valid only at points whose λ^* dots not exceed 18.2, a value that is slightly

TABLE 12. Predicted circumstances at the cornet's encounter with Jupiter in 1994.

Feature identification	Scaled distances λ^*	Radiation pressure accelerations β	Result of encounter with Jupiter
East-northeastern trail	>2.8	All	Miss
and associated tail region	$\leq$2.8	$\leq\beta_{crit}$ [a]	Impacts on July 15-18
	$\leq$2.8	$>\beta_{crit}$ [a]	Miss
Nuclear train	≤ 1 [b]	0	Impacts on July 18-23
and associated tail region	≤ 1 [b]	$\leq\beta_{crit}$ [c]	Impacts on July 18-26
	≤ 1 [b]	$>\beta_{crit}$ [c]	Miss
West-southwestern trail	$\leq$25	0	Impacts on July 23- Ott. 2
and associated tail region	$\leq$25	$\leq\beta_{crit}$ [d]	Impacts on July 23-Ott. 9
	All	$>\beta_{crit}$ [d]	Miss

[a] β_{crit} varies from *0.0029* for $\lambda^* = 2.8$ to 0.00325 at boundary with nuclear train ($\lambda^* = 1$).
[b] By definition.
[c] β_{crit} varies from 0.00325 at eastern end to 0.00365 at western end of train.
[d] β_{crit} varies from *0.00305* at boundary with nuclear train to 0.0086 at trail's adopted endpoint ($\lambda^* = \lambda = 25$).

greater than the trail's adopted length factor in q'able 6. Any particles that may have λ^* larger than this limit will miss Jupiter in] 994. Since the observations suggest that particle accelerations β along this trail increase, apparently linearly, with increasing distance from the nuclear train, a relation $\beta = 0.001023\sim^*$ is implied between the two quantities, as seen from Fig. 11. The impact boundary curve intersects this trail at a point given by $\lambda^* = 2.8$ and $\beta_{crit} = 0.0029$. 'J'his will be the comet's first debris to strike Jupiter, just three days or so before the arrival of the fragment A. The predicted jovigraphic latitude of the first impacts is about +40°, the meridian angle ~50° cast of the local midnight, and the angle between the Earth and the impact site measured from Jupiter's center ~1 15°, so these early events will again take place on the planet's far side.

All the debris distributed along the west-southwestern trail will collide with Jupiter (Fig. 11), but not until after the major fragments. For this trail's adopted length factor $\lambda = 25$ ('1'able 6), the impacts arc predicted to continue for $\sim 2\frac{1}{2}$ months, from late July through early October 1994, and the impact sites to be strongly time dependent. The jovigraphic latitude is expected to be about --sO° in late July, – 60° in the second half of August, back to –45° in mid-September and to --15° at the beginning of October. During the same period of time, the meridian angle is predicted to increase gradually from ~40° all the way to ~1 10" east of the local midnight. On the other hand, the angle subtended by the directions to Earth and to the impact sites, as viewed from the center of Jupiter, is predicted to decrease from ~110° to ~60°. The impact sites will pass from the planet's far side to its near side on August 21, from which time on impacts will be observable from Earth directly, provided the magnitude of these events has reached the detection threshold.

From the critical radiation pressure accelerations β_{crit} of the tail particles it follows that only those larger than ~0 .] to ~1 mm in radius will collide with Jupiter. The impact sites will depend strongly on both the impact time and the particle acceleration β, except for particles sub jected to accelerations near β_{crit}. These will strike the planet on the far side, at a jovigraphic latitude of about +40° and a meridian angle of 45° to 50° east of the local midnight regardless of the impact time; in these cases the angle between the impact point and Earth, measured at Jupiter's center, is 115° to 120°.

Wc have not examined the trails and the tail regions that correspond to scaled distances λ^* larger than the length factors adopted in '1'able 6, because of the expected severe depletion of the particle population. However, all such debris distributed to the northeast of the comet will miss Jupiter in]994, while that confined to a narrow band along the west-southwestern trail will strike the planet during October and the following months.

Even though the fragments and other debris of P/Shoemaker–Levy 9 that will collide with Jupiter occupy an extremely limited volume of space, they contain virtually all the mass of the progenitor cornet, estimated at 7×10^{16} g at an assumed density of 0.2 g/cm^3. A little more than 10% of this mass will be dissipated in the jovian atmosphere by the various components of the brightest fragment during a fcw closely spaced events, probably on July 22, 1994, somewhat more than 80% will be delivered by the 20 remaining fragments during a period of less than 6 days, on July] 8-23,] 994, and the rest, some 5%, by the submillimeter- to subkilometer-sized debris between mid-J uly and early October 1994. Only limited activity might occur before the beginning and/or after the end of this period of time. Much of the microscopic debris, in particular all micron- and suhmicro:k-sized particles (with the exception of extremely tiny grains, *<<0.1 μm in size,* which, if present,

would essentially be unaffected by radiation pressure) will miss not only the planet, but the entire jovian system. The particulate debris that will be injected into the spherical volume of space between the planet and the orbit of Callisto will consist of grains subjected to solar radiation pressure accelerations of $\beta_{crit} < \beta \lesssim 0.04$, whose typical sizes are between several tens of microns and <0.1 cm and which are estimated to carry an extremely small fraction, perhaps on the order of $\lesssim$1 0'0 the comet's mass, or a total of only several tons or less. Proportionately less mass will be injected by the comet into the smaller volumes of space, bounded by the orbits of the satellites interior to Callisto. It is therefore questionable whether this amount **Of** dust will suffice **to** trigger major phenomena in the jovian magnetosphere and/or in the charged environment of Io's torus. If not, any possible disturbance of this type would be due to short-term interactions involving the material about to strike the planet.

Much of what wc have predicted for the fate of comet Shoemaker-Levy 9 is based upon an orbit solution computed from astrometric observations of the train's midpoint. This reference point has no large fragment associated with it nor does it represent the cornet's center of mass. As pointed out in the beginning of Sec. 9, the motion of the midpoint, computed from 1993 observations, will not correspond to its motion in 1994 duc to increasing differential perturbations between the train 's endpoints, In the future, we strongly encourage observers to provide astrometric observations Of *individual* fragments with respect to background stars. Astrometric observations for all the fragments would be very helpful in predicting the train's evolution. However, since the predicted relative positions of the fragments arc likely to be more accurately determined than their individual inertial positions, astrometric observations of only a few of the brighter fragments will improve the position accuracy for all of them. In addition, we encourage observers to provide position angle and angular separation observations for individual fragments with respect to the brightest fragment.

Our investigation describes and interprets the complex character of the processes responsible for the highly unusual appearance of P/Shoemaker-Levy 9 and provides information on the various phenomena expected during the comet's forthcoming encounter with Jupiter. Even though it is obvious that for all practical purposes the comet will cease to exist in 1994, much of its finer debris will escape the doomed fate of the large fragments and will also avoid any interaction with the jovian magnetosphere and 10's torus. Most of the microscopic debris will apparently end up in widely scattered orbits controlled by a continuing tug of war between the gravitational fields of Jupiter and the Sun.

Wc thank 1). Jewitt for communicating his astrometric measurements of the individual fragments on the comet's images taken by himself, J. Luu, and J. Chen. We also thank 11. A. Weaver for in-depth information on the images obtained with the Hubble Space Telescope and J. V. Scotti for providing us with the image of P/Shoemaker-Levy 9 which is reproduced in Fig. 1. We arc grateful to E.F. Helin and W. Z. Wisniewski for informing us on their images of the comet, which we used for feature measurements reported in Table 2. 'l'his research was carried out by the Jet]'repulsion laboratory, California Institute of Technology, under contract with the National Aeronautics and Space Administration. Partial support was provided by NASA through Grant GO-5021 .01-92A from the Space Telescope Science Institute, which is operated by the Association of Universities for Research in Astronomy, Inc.

REFERENCES

Aggarwal, H. R., and Oberbeck, V. R. (1974), Astrophys. J., 191, 577.

Bailey, M. E., Clube, S. V. M., and Napier, W. M. (] 99o), *The Origin of Comets* (Pergamon, Oxford), 577 pp.

Bortle, J. E. (1 993), IAU Circ. No. 5766.

Cavagna, M., Gualdoni, C., Sicoli, P., and Testa, A. (1993), Minor Planet Circ. No. 21988.

Dobrovolskis, A. R. (1990), Icarus, 88, 24.

Dobrovolskis, A. R., and Burns, J. A. (1984), Icarus, 57, 464.

Feldman, P. I)., Festou, M. C., A'Hearn, M. F., Arpigny, C., Butterworth, P. S., Cosmovici, C. B., Danks, A. C., Gilmozzi, R., Jackson, W. M., McFadden, 1,. A., Patriarchi, 1'., Schleicher, D. G., Tozzi, G. P., Wallis, M. K., Weaver, H. A., and Woods, T. N. (1987), Astron. Astrophys., 187, 325.

Green, D. W. E., ed. (1993), Internat. Comet Q., 15, 63, 100, 106, 136, ant] 181.

Hartmann, W. K. (]978), Icarus, 33, 50.

Helin, E. F. (1 993), private communication.

Jewitt, 1). (1993), private communication,

Keller, H. U. *et al.* (1987), Astron. Astrophys., 187, 807.

Mclosh, H. J., and Schenk, P. (1993), Nature, 365, 731.

Meyer, E., Obermair, E., and Raab, H. (1993), Minor Planet Circ. Nos. 21988, 22120, 22121, 22283, and 22284.

Osgood, W. F. (1 949), *Mechanics*, Macmillan, Ncw York, pp. 275-276.

Rickman, H. (1986), in The Comet Nucleus Sample Return Mission, ESA SF'- 249, edited by O. Melita (ESTEC, Noordwijk), p. 195.

Scotti, J. V. (1993), IAU Circ. Nos. 5725 and 5745; Minor Planet Circ. Nos., 21987, 21988, and 22283.

Scotti, J. V., and Melosh, H. J. (1993), Nature, 365, 733.

Seidelmann, P. K., cd. (1 992), *Explanatory Supplement to the Astronomical Almanac*, University Science Books, Mill Valley, CA, p. 404.

Sekanina, Z. (1977), Icarus, 30, 574.

Sekanina, Z. **I(I 981),** Annu. Rev. Earth Planet. Sci., 9, 113.

Sekanina, Z. 1(1991), Astron. J., 102, 1870.

Sekanina, Z. 1(1993), Science, 262, 382.

Standish, E. M. (1990), Astron. Astrophys., 233, 252.

Sykes, M. V., Lien, D. J., and Walker, R. G. (1990), Icarus, 86, 236.

Sykes, M. V., and Walker, R. G. (1992), Icarus, 95, 180.

Urata, '1'. (1 993), Minor Planet Circ. No. 21989.

Weaver, H. A. *et al.* (1 993), Science, submitted.

Wisnicwski, W. Z. (1 993), private communication.

Wyckoff, S., 'Wagner, R. M., Wehinger, P. A., Schleicher, I). G., and Festou, M. C. (1985), Nature, 316, 241.